

Geology of the Northern Norrbotten ore province, northern Sweden

Paper 7 (13)

Editor: Stefan Bergman



SGU

Sveriges geologiska undersökning
Geological Survey of Sweden

Rapporter och meddelanden 141

Geology of the Northern Norrbotten ore province, northern Sweden

Editor: Stefan Bergman

Sveriges geologiska undersökning
2018

ISSN 0349-2176
ISBN 978-91-7403-393-9

Cover photos:

Upper left: View of Torneälven, looking north from Sakkaravaara, northeast of Kiruna. **Photographer:** Stefan Bergman.

Upper right: View (looking north-northwest) of the open pit at the Aitik Cu-Au-Ag mine, close to Gällivare. The Nautanen area is seen in the background. **Photographer:** Edward Lynch.

Lower left: Iron oxide-apatite mineralisation occurring close to the Malmberget Fe-mine. **Photographer:** Edward Lynch.

Lower right: View towards the town of Kiruna and Mt. Luossavaara, standing on the footwall of the Kiruna apatite iron ore on Mt. Kiirunavaara, looking north. **Photographer:** Stefan Bergman.

Head of department, Mineral Resources: Kaj Lax

Editor: Stefan Bergman

Layout: Tone Gellerstedt och Johan Sporrang, SGU

Print: Elanders Sverige AB

Geological Survey of Sweden
Box 670, 751 28 Uppsala
phone: 018-17 90 00
fax: 018-17 92 10
e-mail: sgu@sgu.se
www.sgu.se

Table of Contents

Introduktion (in Swedish)	6
Introduction	7
1. Regional geology of northern Norrbotten County	9
References	14
2. Geology, lithostratigraphy and petrogenesis of c. 2.14 Ga greenstones in the Nunasvaara and Masugnsbyn areas, northernmost Sweden	19
Abstract	19
Introduction	20
Regional setting of Norrbotten greenstone belts	21
Geology of the Nunasvaara and Masugnsbyn greenstone successions	23
Petrogenesis of the greenstones: Preliminary U-Pb geochronology, litho-geochemistry and Sm-Nd isotopic results	52
Summary and conclusions	68
Acknowledgements	69
References	70
3. Stratigraphy and ages of Palaeoproterozoic metavolcanic and metasedimentary rocks at Käymäjärvi, northern Sweden	79
Abstract	79
Introduction	80
General geology	80
Structure and stratigraphy of the Käymäjärvi area	81
Sample description	89
Analytical methods	90
Analytical results	91
Discussion	96
Conclusions	100
Acknowledgements	101
References	101
4. Petrological and structural character of c. 1.88 Ga meta-volcanosedimentary rocks hosting iron oxide-copper-gold and related mineralisation in the Nautanen–Aitik area, northern Sweden	107
Abstract	107
Introduction	108
Regional setting	108
Geology of the Nautanen–Aitik area	110
Structural geology and deformation	132
Summary and Conclusions	144
Acknowledgements	144
References	145
5. Age and lithostratigraphy of Svecofennian volcanosedimentary rocks at Masugnsbyn, northernmost Sweden – host rocks to Zn-Pb-Cu- and Cu ±Au sulphide mineralisations	151
Abstract	151
Introduction	152
Geological overview	153
Discussion and preliminary conclusions	194
Acknowledgements	197
References	198

6. Folding observed in Palaeoproterozoic supracrustal rocks in northern Sweden	205
Abstract	205
Introduction	205
Geological setting	207
Structural geological models	209
Geophysical data	212
Discussion and Conclusions	251
References	255
7. The Pajala deformation belt in northeast Sweden:	
Structural geological mapping and 3D modelling around Pajala	259
Abstract	259
Geological setting	259
Structural analysis	263
2D regional geophysical modelling and geological interpretation	272
Local and semi-regional 3D models	274
Discussion	280
Conclusions	283
References	284
8. The Vakko and Kovo greenstone belts north of Kiruna:	
Integrating structural geological mapping and geophysical modelling	287
Abstract	287
Introduction	287
Geological setting	289
Geophysical surveys	291
Results	296
Discussion	306
Conclusions	308
References	309
9. Geophysical 2D and 3D modelling in the areas around	
Nunasvaara and Masugnsbyn, northern Sweden	311
Abstract	311
Nunasvaara	312
2D modelling of profile 1 and 2	316
Masugnsbyn	321
Regional modelling	329
Conclusion	338
References	339
10. Imaging deeper crustal structures by 2D and 3D modelling of geophysical data.	
Examples from northern Norrbotten	341
Abstract	341
Introduction	341
Methodology	342
Geological setting	342
Results	345
Conclusion	358
Outlook	358
Acknowledgements	358
References	359

11. Early Svecokarelian migmatisation west of the Pajala deformation belt, northeastern Norrbotten province, northern Sweden	361
Abstract	361
Introduction	362
Geology of the Masugnsbyn area	362
Discussion	372
Conclusions	374
Acknowledgements	375
References	376
12. Age and character of late-Svecokarelian monzonitic intrusions in northeastern Norrbotten, northern Sweden	381
Abstract	381
Introduction	381
Geological setting	382
Analytical methods	387
Analytical results	388
Discussion	393
Conclusions	396
Acknowledgements	396
References	397
13. Till geochemistry in northern Norrbotten –regional trends and local signature in the key areas	401
Abstract	401
Introduction	401
Glacial geomorphology and quaternary stratigraphy of Norrbotten	403
Samples and methods	406
Results and discussion	407
Conclusions	426
Acknowledgements	427
References	427

Introduktion

Stefan Bergman & Ildikó Antal Lundin

Den här rapporten presenterar de samlade resultaten från ett delprojekt inom det omfattande tvärvetenskapliga Barentsprojektet i norra Sverige. Projektet initierades av Sveriges geologiska undersökning (SGU) som ett första led i den svenska mineralstrategin. SGU fick ytterligare medel av Näringsdepartementet för att under en fyraårsperiod (2012–2015) samla in nya geologiska, geofysiska och geokemiska data samt för att förbättra de geologiska kunskaperna om Sveriges nordligaste län. Det statligt ägda gruvbolaget LKAB bidrog också till finansieringen. Projektets strategiska mål var att, genom att tillhandahålla uppdaterad och utförlig geovetenskaplig information, stödja prospekterings- och gruvindustrin för att förbättra Sveriges konkurrenskraft inom mineralnäringen. Ny och allmänt tillgänglig geovetenskaplig information från den aktuella regionen kan hjälpa prospekterings- och gruvföretag att minska sina risker och prospekteringskostnader och främjar därigenom ekonomisk utveckling. Dessutom bidrar utökad geologisk kunskap till en effektiv, miljövänlig och långsiktigt hållbar resursanvändning. All data som har samlats in i projektet lagras i SGUs databaser och är tillgängliga via SGU.

Syftet med det här delprojektet var att få en djupare förståelse för den stratigrafiska uppbyggnaden och utvecklingen av de mineraliserade ytbergarterna i nordligaste Sverige. Resultaten, som är en kombination av ny geologisk kunskap och stora mängder nya data, kommer att gynna prospekterings- och gruvindustrin i regionen i många år framöver.

Norra Norrbottens malmprovins står för en stor del av Sveriges järn- och kopparmalmsproduktion. Här finns fyra aktiva metallgruvor (mars 2018) och mer än 500 dokumenterade mineraliseringar. Fyndigheterna är av många olika slag, där de viktigaste typerna är stratiforma kopparmineraliseringar, järnformationer, apatitjärnmalm av Kirunatyp och epigenetiska koppar-guldmineraliseringar. En vanlig egenskap hos de flesta malmer och mineraliseringar i Norr- och Västerbotten är att de har paleoproterozoiska vulkaniska och sedimentära bergarter som värdbergart. För undersökningarna valdes ett antal nyckelområden med bästa tillgängliga blottningsgrad. De utvalda områdena representerar tillsammans en nästan komplett stratigrafi i ytbergarter inom åldersintervallet 2,5–1,8 miljarder år.

Rapporten består av tretton kapitel och inleds med en översikt över de geologiska förhållandena, som beskriver huvuddragen i de senaste resultaten. Översikten följs av fyra kapitel (2–5) som huvudsakligen handlar om litostratigrafi och åldersbestämningar av ytbergarterna. Huvudämnet för de därpå följande fem kapitlen (6–10) är 3D-geometri och strukturell utveckling. Därefter kommer två kapitel (11–12) som fokuserar på U-Pb-datering av en metamorf respektive intrusiv händelse. Rapporten avslutas med en studie av geokemin hos morän i Norra Norrbottens malmprovins (kapitel 13).

Introduction

Stefan Bergman & Ildikó Antal Lundin

This volume reports the results from a subproject within the Barents Project, a major programme in northern Sweden. The multidisciplinary Barents Project was initiated by SGU as the first step in implementing the Swedish National Mineral Strategy. SGU obtained additional funding from the Ministry of Enterprise and Innovation to gather new geological, geophysical and till geochemistry data, and generally enhance geological knowledge of northern Sweden over a four-year period (2012–2015). The state-owned iron mining company LKAB also helped to fund the project. The strategic goal of the project was to support the exploration and mining industry, so as to improve Sweden's competitiveness in the mineral industry by providing modern geoscientific information. Geological knowledge facilitates sustainable, efficient and environmentally friendly use of resources. New publicly available geoscientific information from this region will help exploration and mining companies to reduce their risks and exploration costs, thus promoting economic development. All data collected within the project are stored in databases and are available at SGU.

This subproject within the Barents Project aims to provide a deeper understanding of the stratigraphy and depositional evolution of mineralised supracrustal sequences in northernmost Sweden. The combined results in the form of new geological knowledge and plentiful new data will benefit the exploration and mining industry in the region for many years to come.

The Northern Norrbotten ore province is a major supplier of iron and copper ore in Sweden. There are four active metal mines (March 2018) and more than 500 documented mineralisations. A wide range of deposits occur, the most important types being stratiform copper deposits, iron formations, Kiruna-type apatite iron ores and epigenetic copper-gold deposits. A common feature of most deposits is that they are hosted by Palaeoproterozoic metavolcanic or metasedimentary rocks. A number of key areas were selected across parts of the supracrustal sequences with the best available exposure. The areas selected combine to represent an almost complete stratigraphic sequence.

This volume starts with a brief overview of the geological setting, outlining some of the main recent achievements. This is followed by four papers (2–5) dealing mainly with lithostratigraphy and age constraints on the supracrustal sequences. 3D geometry and structural evolution are the main topics of the next set of five papers (6–10). The following two contributions (11–12) focus on U-Pb dating of a metamorphic event and an intrusive event, respectively. The volume concludes with a study of the geochemical signature of till in the Northern Norrbotten ore province (13).

Authors, paper 7:

Stefan Luth

Geological Survey of Sweden,
Department of Mineral Resources,
Uppsala, Sweden

Cecilia Jönsson

Geological Survey of Sweden,
Department of Mineral Resources,
Uppsala, Sweden

Johan Jönberger

Geological Survey of Sweden,
Department of Mineral Resources,
Uppsala, Sweden

Susanne Grigull

Geological Survey of Sweden,
Department of Physical Planning,
Uppsala, Sweden

Robert Berggren

Geological Survey of Sweden,
Department of Mineral Resources,
Uppsala, Sweden

Bart van Assema

VU University Amsterdam,
Amsterdam, the Netherlands

Willem Smoor

VU University Amsterdam,
Amsterdam, the Netherlands

Thomas Djuly

VU University Amsterdam,
Amsterdam, the Netherlands

7. The Pajala deformation belt in northeast Sweden: Structural geological mapping and 3D modelling around Pajala

Stefan Luth, Cecilia Jönsson, Johan Jönberger, Susanne Grigull, Robert Berggren, Bart van Assema, Willem Smoor & Thomas Djuly

ABSTRACT

Results from structural geological mapping and 3D geological subsurface modelling of the Palaeoproterozoic Pajala deformation belt (PDB) in northeast Sweden are presented. The structural geological map is based on integration between detailed geological field observations and interpreted geophysical datasets (magnetic, electromagnetics and gravity). The deformation pattern obtained reveals a complex network of several parallel and intersecting shear zones striking mainly N–S and bounding tightly-folded domains. Strike and dip measurements and sense of shear determinations on these mapped structures were then combined with the subsurface geometries obtained from 2D and 3D models based on gravity, magnetic and electromagnetic data. The resulting 3D geological interpretation yields a wedge-shaped subsurface geometry for the Pajala deformation belt with steeply east-dipping shear zones along its western border and steeply west-dipping shear zones towards the east. Internally, the wedge is folded into multiple ellipsoidal dome structures bounded by a network of N–S-striking shear zones. The folded domes appear strongly elongated in a N–S direction, suggesting E–W flattening and possible vertical extrusion as the main deformation mechanisms. Tectonically, the PDB is now interpreted as a 60 to 80 km wide transpressive wedge formed during NE–SW transpressive shortening (D1), followed by E–W shortening (D2). An eastward offset of the PDB along the intersecting NE–SW-striking Kolari shear zone north of Pajala probably occurred during D2. Relatively young metamorphic ages (1.8 Ga) recorded in the PDB in relation to its surroundings (1.84 Ga) indicate that D2, which (re)folded the main metamorphic fabric in the PDB, must have occurred after 1.8 Ga. Finally, deformation by NNW–SSE shortening (D3) caused discrete faulting and sinistral brittle-ductile reactivation, mainly along the western boundary of the PDB.

GEOLOGICAL SETTING

The Pajala deformation belt

The Pajala deformation belt (PDB) is a large N–S-trending high-strain belt transecting the Fennoscandian Shield from the Baltic Sea into northern Sweden, Finland and Norway. The belt was formerly named the Baltic–Bothnian megashear by Berthelsen & Marker (1986), and was interpreted to

have resulted from large intraplate strike-slip movements. Kärki et al. (1993) renamed the belt the Pajala Shear Zone and assigned a prominent dextral strike-slip component to it. More recently, contrasting plate kinematic models were proposed by Nironen et al. (1997) and Lahtinen et al. (2005, 2015), suggesting the PDB was formed during continental rifting, or was a suture zone, respectively. In both scenarios the PDB accommodated dextral and sinistral movements during stages of subsequent reactivation. The evidence for these tectonic interpretations is primarily based on large-scale geophysical patterns as well as geochronological data derived from the major lithotectonic units surrounding the PDB (Lahtinen et al. 2015). However, no detailed structural geological study has been carried out along the Swedish part of the PDB, nor have any attempts been made to unravel its subsurface geometries in 3D. The existing tectonic models must therefore be examined in light of the outcomes from an integrated, structurally-orientated, geological study along the PDB.

This study focuses on the Swedish part of the PDB, striking along the border with Finland (Fig. 1). To the south of the small town of Pajala, the belt is up to 60 km wide and comprises several N–S-striking parallel shear zones mainly interpreted from airborne magnetic and gravity surveys (Fig. 2). North of Pajala, however, the PDB is intersected by the NE–SW-striking Kolari shear zone, causing an apparent eastward bending of the PDB into Finland (Väisänen 2002, Niiranen et al. 2007). As such, the PDB and Kolari shear zone were lumped together as the Kolari–Pajala Shear Zone in studies focusing on the Finnish side (e.g. Niiranen et al. 2009, Niiranen 2011). Detailed investigations in Finland based on mapping and depth interpretations along a seismic profile crossing the Kolari–Pajala shear zone (Fig. 4B) revealed several shear zones with different orientations (Niiranen 2011). It is evident from these studies that the observed deformation pattern reflects multiple phases of deformation. Earlier geological studies and mapping projects focusing on the Swedish section also recognised that deformation within, as well as outside, the PDB was polyphase, resulting in superimposed and interfering folding patterns (Eriksson 1954, Padget 1977, Grigull et al. 2018). It has been suggested by the same authors that major northwest–southeast-trending folds (F1) became refolded by north–south-trending F2 folds. Refolding by F2 was most intense within the PDB and intimately associated with shearing along the N–S-orientated shear zones, resulting in the formation of tectonic lenses composed of folded gneisses, migmatites or more massive granitoids. Eastern-side-up sense of shear documented along the western boundary of the PDB was proposed in previous studies to explain major east–west jump in the grade and timing of metamorphism (Bergman et al. 2001, 2006, Jonsson and Kero 2013). West of this boundary, upper greenschist facies metamorphism is recorded at 1.85 Ga, whereas units inside the PDB underwent upper amphibolite facies metamorphism between 1.82 and 1.78 Ga. Apart from observations at one locality (Bergman et al. 2001), structural geological evidence to support eastern-side-up movements is still lacking, but was one of the aims of this study. Moreover, the PDB largely overlaps the Fe–Cu–Au Pajala–Kolari metallogenic area. Studies on deposits located on the Finnish side of the PDB indicated an iron oxide–copper–gold (IOCG) affinity as well as large structural control by major shear zones and more locally by second to fourth-order shear zones and faults (e.g. Niiranen et al. 2007). An improved understanding of deformation history and the resulting structural pattern in the bedrock around the town of Pajala is therefore crucial to better constrain the region's ore potential.

Lithostratigraphy and deformation in the Pajala area

The Pajala region is predominantly made up of Palaeoproterozoic supracrustal rocks (2.4–1.86 Ga) and intrusive rocks related to several magmatic suites (1.96–1.75 Ga, Fig. 1). Most of the rocks were formed in a volcanic arc setting and were deformed and metamorphosed during the Svecokarelian orogeny (Bergman et al. 2001). The study area is subdivided into three domains based on distinctive lithology, deformation pattern or metamorphic grade (Fig. 1). The *greenstone domain* north of Pajala is composed of rocks mainly belonging to the Karelian greenstone group (2.3–1.96 Ga); the *migmatite domain*,

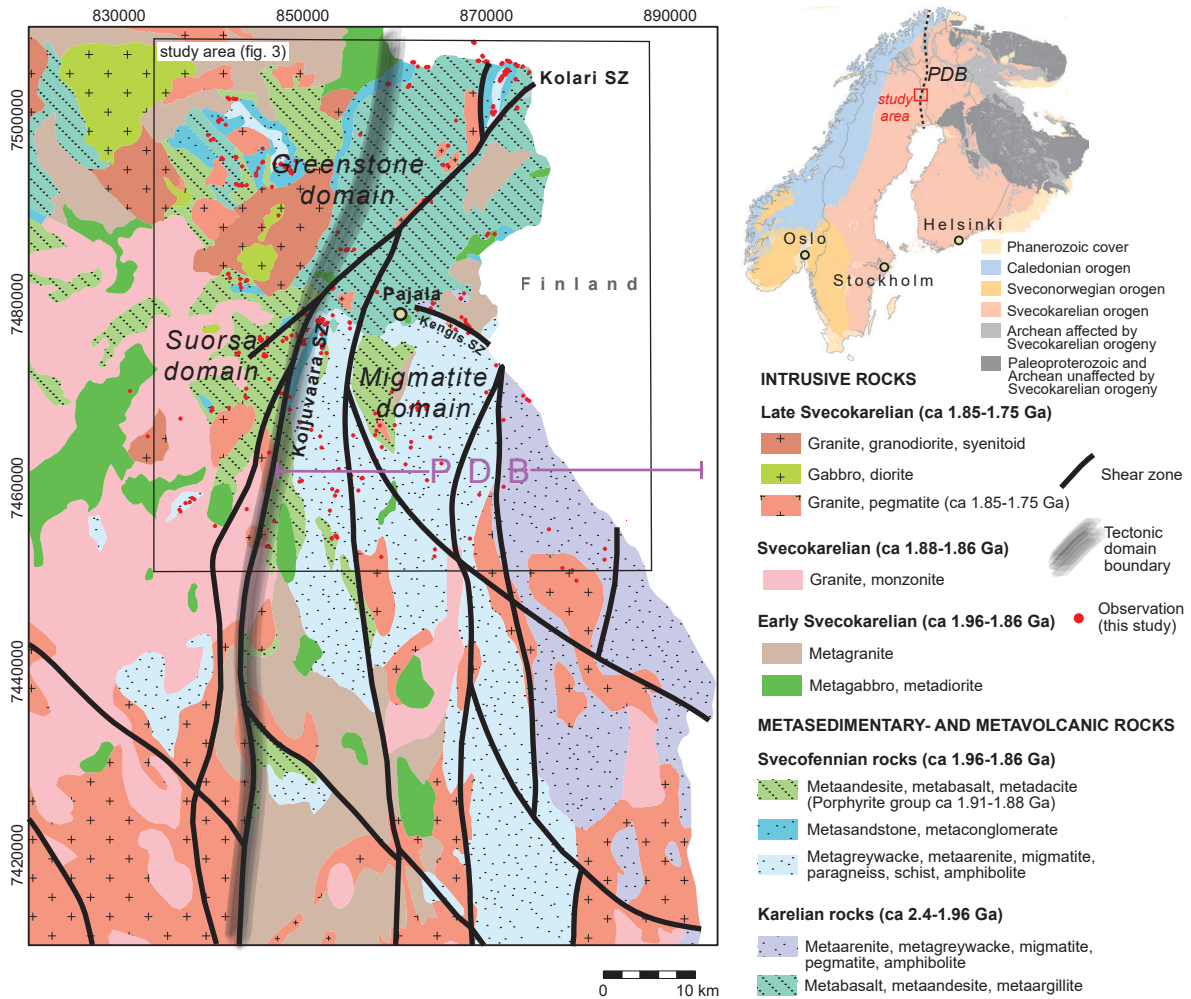


Figure 1. Geological map of the Pajala area. PDB: Pajala deformation belt, SZ: shear zone. Only the major shear zones are displayed on this map and are derived mainly from geophysical data. The tectonic domain boundary (thick black line) is based on Bergman et al. (2006). Figure 3 shows a more detailed and complete structural map of the study area. Insert map shows the main geological domains of the Fennoscandian shield.

south of Pajala, is characterised by strongly deformed metasedimentary rocks of Svecofennian age (1.96–1.88 Ga); and the *Suorsa Domain*, directly west of the PDB, is composed of weakly deformed mafic to intermediate metavolcanic rocks of roughly the same age as the metasedimentary rocks.

The predominant rock types in the greenstone domain are mafic and ultramafic pyroclastic and volcanoclastic rocks. Higher up in the stratigraphy, mafic tuffites intercalated by graphitic layers, carbonates and iron-rich sedimentary rocks (BIF) occur. The overlying 200 m thick dolomite unit hosts economically important skarn iron ore deposits: Stora Sahavaara, Runtijärvi, Tapuli and Palotieva. Based on the abundance of garnet and diopside, the metamorphic grade in the greenstone domain reached at least amphibolite facies. Scapolite alteration affecting mafic rocks is common and locally very strong (Grigull & Berggren 2015). Due to very limited bedrock exposures, structural data north of Pajala was mainly obtained for this study from the Ristimilla and Käymäjärvi areas. For a more detailed description of the Karelian greenstone group the reader is referred to Padget (1977), Martinsson & Wanhainen (2013) and Martinsson et al. (2018).

The Migmatite domain is characterised by metaarenites, metagreywackes and banded gneisses, which are mostly migmatitic. Detrital zircon studies on the metaarenite yield mostly 1.91 Ga inherited

grains (Bergman et al. 2001, Lahtinen et al. 2015, Ladenberger et al., 2018). These rocks underwent amphibolite facies metamorphism with peak temperatures of between 510–615 °C at 4–6 kbar around 1.8 Ga (Bergman et al. 2006). Some common metamorphic minerals present include sillimanite, cordierite and garnet. Despite the high-grade metamorphism, sedimentary structures such as cross-bedding are locally well preserved. In the western part of the Migmatite domain in particular, the metamorphic grade is highly variable. Within the well-preserved sedimentary rocks, Martinsson et al. (2004) documented ripple marks, indicating a shallow marine depositional environment for the Sammakkoara group. In contrast, areas with predominantly diatexitic migmatites show an enrichment of granitic and pegmatitic material. Locally, granitic intrusions occur as elongated bodies aligned with shear zones. These rocks are weakly foliated to massive pinkish granite, pegmatite or aplites, and are characterised by a relatively high radium index (0.8). Foliated units are commonly intruded or brecciated by pegmatite, indicating multiple injection events along the PDB.

The Suorsa domain is predominantly composed of mafic to intermediate metavolcanic rocks, which were also included in the Sammakkoara group by Martinsson et al. (2004), albeit occurring on a higher stratigraphic level than the metasedimentary rocks from the Migmatite domain. The metavolcanic rocks are generally fine-grained and contain hornblende and plagioclase phenocrysts with some pyrite, epidote and magnetite. Laminated tuffs and volcanic breccias occur locally. The volcanic rocks are of an andesitic to trachyandesitic composition and a calc-alkaline signature, interpreted as reflecting arc-volcanism during northeastward subduction of oceanic crust below an Archaean palaeocontinent (Martinsson et al. 2004). The deformation imprint varies from very weakly deformed rocks to locally intensively sheared mylonites and associated discrete shear zones. The metamorphic grade in the Suorsa domain is predominantly lower to upper greenschist facies, but reaches amphibolite facies in a few areas with predominantly by metasedimentary rocks. The volcanic rocks are dated at 1.88 Ga by Martinsson et al. (2018).

Geophysical characterisation

The Pajala region is well covered by geophysical measurements, with a complete coverage of gravity, airborne magnetic, gamma-ray spectrometry and electromagnetic measurements (VLF and slingram) (Fig. 2A, B and Luth & Jönsson (2014), Grigull et al. (2014)). The spatial distribution of gravity measurements is approximately one point per 1.5 km², but measurement locations are locally more closely spaced. For a detailed overview on the different types and coverage of the geophysical datasets in the study area the reader is referred to Luth & Jönsson (2014).

Within the study area, the gravitational field shows two distinctive negative anomalies (Fig. 2A). One correlates with the low density quartz-feldspar rich paragneiss in the Migmatite domain; the other is found in the northwestern corner of the study area. Positive Bouguer anomalies correlate with rocks with basaltic to andesitic composition in the Suorsa and Migmatite domains. The Migmatite domain shows a homogeneous low-magnetic pattern in the west and somewhat higher magnetism in the east. Low magnetic anomalies were identified with an N–S ellipsoidal-shaped outline, some of which have been subject to structural and 3D modelling studies. The Migmatite domain can also be distinguished in the electromagnetic anomaly pattern, in which increased electrical conductivity is observed in the in-phase component. The magnetic pattern for the Suorsa domain varies considerably, with areas of high or low-magnetic signature, anomalies reflecting fold patterns, as well as disrupted anomalies due to intense deformation and shearing within the PDB.

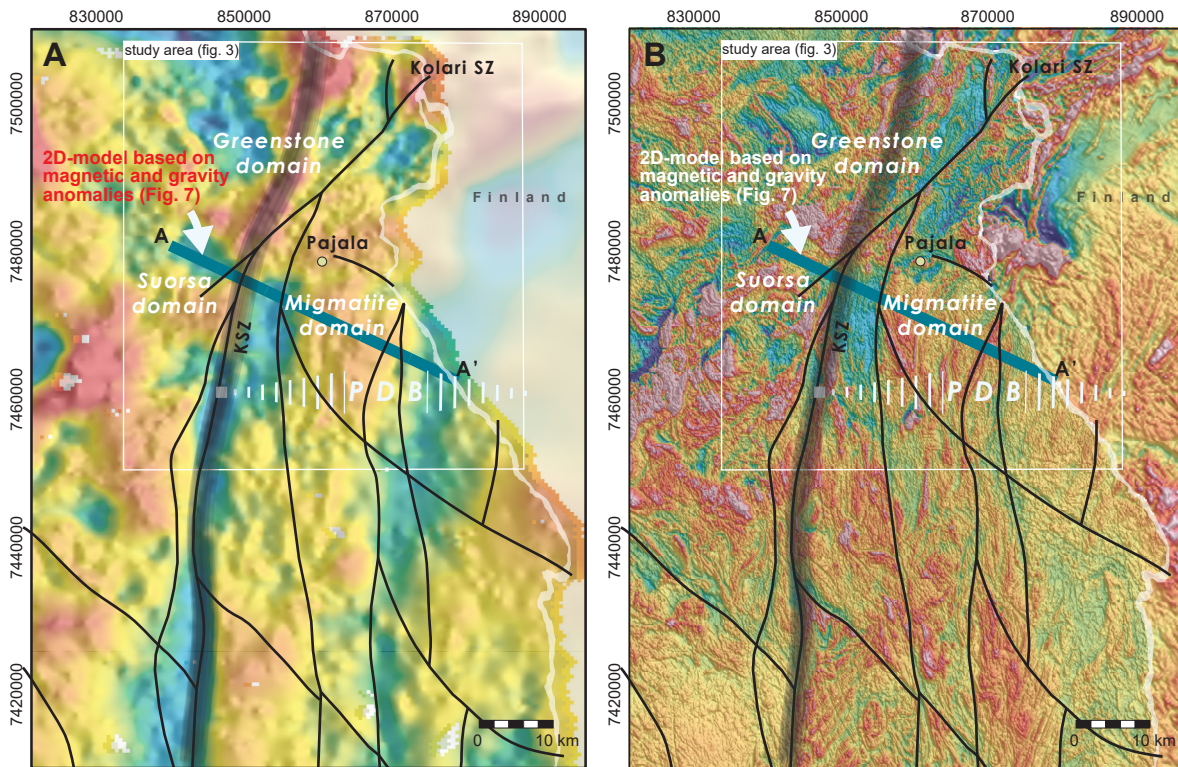


Figure 2. Geophysical anomaly maps of the Pajala area. **A.** Bouguer gravity anomaly map. Blue indicates low gravity anomaly and red indicates high gravity anomaly. **B.** Airborne magnetic anomaly map. Blue indicates low magnetic anomaly and red indicates high magnetic anomaly. Profile line A-A' shown refers to the modelled profile displayed in Figure 7. Shear zones (lines); see the legend in Figure 1. PDB: Pajala deformation belt, KSZ: Koijuvaara shear zone.

STRUCTURAL ANALYSIS

Shear sense indicators and inferred direction of regional shortening

Several directions of shortening were deduced from the analyses of shear sense indicators in the field and in thin section. Figure 3 and Table 1 include the most representative kinematic indicators observed, as well as the inferred directions of shortening under which they may have been formed. Most of the analyses were carried out along shear zones where deformation and shearing were observed in most rock types. However, shear indicators such as asymmetric shear folds, shear bands, mica-fish and sigmoids are generally best developed within banded paragneiss, mica-schist and migmatite, which are the most common rock types in the Migmatite domain. Virtually all shear indicators are observed in a metamorphic fabric (banding, porphyroblasts etc.), and therefore record deformation that most likely post-dates peak metamorphism and migmatitisation.

The structural fabrics seen in outcrops and thin sections often reveal deformation by dextral shearing along N–S-striking and sub-vertically-dipping foliations. In the Migmatite domain in particular, dextral shearing was most commonly observed and is often associated with a medium-grade mylonitic fabric (Fig. 4). The documented dextral shear along a N–S-striking fabric mostly likely developed during NE–SW transpression. Some other shear indicators observed throughout the study area are more consistent with E–W-directed shortening. Additional evidence for E–W shortening in the Migmatite domain is inferred from the pattern of upright folds along N–S-trending fold axes. In the Suorsa domain, E–W shortening was primarily deduced from the predominantly dextral shear sense associated with the NE–SW-striking Kolari Shear Zone. Whether the inferred NE–SW and E–W directions of shortening reflect two separate shortening events or may be considered the result of local strain partitioning is discussed later in this chapter. A third direction of shortening is orientated

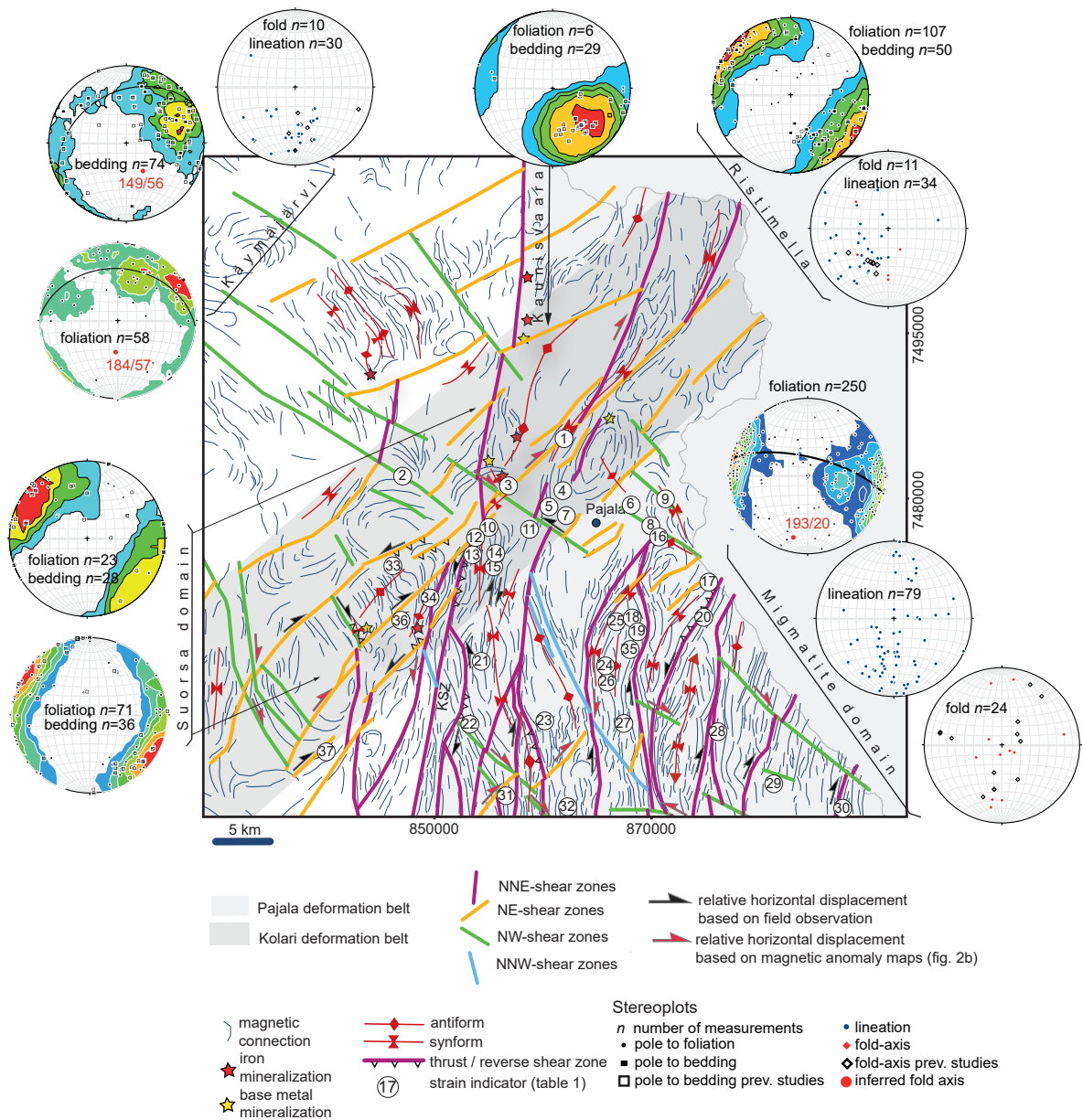


Figure 3: Structural geological map of the Pajala area based on new and existing field data. Numbers refer to the locations of strain indicators observed in outcrops and thin sections (see also Table 1). Notice the distinction made between two intersecting deformation belts as the main difference when compared with previous published maps (Fig. 1).

Table 1. Location and type of observed strain indicators as displayed in Figure 3.

Nr (Fig. 3)	North (Sweref 99)	Easting (Sweref 99)	Domain	Lithology	Strain indicator	Kinematics	Inferred direction of shortening
1	7485784	857942	Greenstone	paragneiss	drag fold	sinistral	NW-SE
2	7482491	843671	Greenstone	igneous rock	rotated clast	reverse, top-to-the-NNW	NW-SE
3	7481670	853029	Greenstone	BIF	upright fold		ENE-WSW
4	7481191	857787	Greenstone	migmatite	fold (F2)		E-W
5	7479358	856206	Greenstone	paragneiss	fault	sinistral	ENE-WSW
5	7479358	856206	Greenstone	paragneiss	fold (F1)		NE-SW
6	7479944	863843	Greenstone	paragneiss	garnet porphyroblast	dextral	NE-SW
7	7479250	856318	Greenstone	paragneiss	sigmoid	sinistral	ENE-WSW
8	7478158	865552	Greenstone	paragneiss	fold (F1)		NE-SW
8	7478158	865552	Greenstone	paragneiss	fold (F2)		E-W

Table 1 continues

Nr (Fig. 3)	North (Sweref 99)	Easting (Sweref 99)	Domain	Lithology	Strain indicator	Kinematics	Inferred direction of shortening
9	7480482	866899	Greenstone	paragneiss	shear band	dextral	NW-SE
10	7477973	851256	Migmatite	micaschist	CS, mica fish	sinistral	NNW-SSE
10	7477973	851256	Migmatite	micaschist	CS, mica fish	dextral-reverse	NE-SW
11	7477835	854824	Migmatite	paragneiss	drag fold	dextral	N-S
12	7477054	850102	Migmatite	paragneiss	drag fold	sinistral	N-S
13	7475601	849810	Migmatite	paragneiss	CS, mica-fish	reverse	E-W
14	7475422	851744	Migmatite	paragneiss	CS, mica-fish	dextral	NE-SW
15	7475138	851810	Migmatite	paragneiss	shear band	dextral	NE-SW
16	7477150	866319	Migmatite	paragneiss	fold (F1)		NE-SW
17	7473207	870709	Migmatite	paragneiss	mica-fish	dextral	NE-SW
17	7473207	870709	Migmatite	paragneiss	mica-fish	reverse (top-to-the-ESE)	E-W
18	7468812	863312	Migmatite	migmatite	fold (F2)		E-W
19	7468820	863008	Migmatite	migmatite	thrust	reverse (top-to-the-NNE)	NNE-SSW
20	7470069	870243	Migmatite	paragneiss	drag fold	sinistral	NW-SE
21	7466229	850611	Migmatite	migmatite	drag fold	sinistral	NW-SE
22	7460694	849576	Migmatite	paragneiss	rotated clast	dextral	NE-SW
22	7460694	849576	Migmatite	paragneiss	sigmoid	reverse (top-to-the-W)	NE-SW
23	7460963	856205	Migmatite	paragneiss	drag fold	sinistral	NW-SE
24	7464914	861486	Migmatite	paragneiss	fold (F2)		E-W
25	7468477	863131	Migmatite	paragneiss	garnet porphyroblast	dextral	NE-SW
26	7464301	861444	Migmatite	migmatite	drag fold	dextral	NE-SW
27	7460711	863213	Migmatite	paragneiss	sigmoid	reverse (top-to-the-E)	E-W
28	7460016	871530	Migmatite	paragneiss	sigmoid	sinistral	NW-SE
29	7455418	876425	Migmatite	paragneiss	sigmoid	dextral	NE-SW
30	7453245	882560	Migmatite	paragneiss	drag fold	sinistral	NE-SW
31	7454418	852819	Migmatite	metagranite	fold		E-W
32	7452408	858216	Migmatite	paragneiss	drag fold	dextral	NE-SW
33	7474601	842747	Suorsa	andesite	sigmoid	dextral	E-W
33	7474601	842747	Suorsa	andesite	conjugate faults		NNW-SSE
34	7471759	846047	Suorsa	andesite	drag fold	dextral	E-W
35	7468477	863131	Suorsa	biotite gneiss	drag fold	dextral	NE-SW
35	7468477	863131	Suorsa	biotite gneiss	reverse fault	reverse (top-to-the-W)	E-W
36	7469807	843451	Suorsa	altered rock	sigmoid	dextral	ENE-WSW
37	7458252	836943	Suorsa	paragneiss	sigmoid	dextral	WNW-ESE

NNW–SSE and is inferred from shear sense indicators along brittle-ductile shear zones in the Migmatite domain and conjugate faults in the Suorsa domain. Typically, the NW–SE-orientated brittle-ductile shear zones and faults accommodated dextral slip, while the intersecting NE–SW-orientated zones generally record sinistral slip. Moreover, only a few shear indicators were observed in vertical sections and mostly indicated E–W flattening or reverse shearing. As such, eastern-side-up shearing along a steeply eastward-dipping fabric was recorded southwest of Pajala, whereas in the eastern part of the Migmatite domain western-side-up shearing along steeply westward-dipping structures was observed.

Structural geological map of the Pajala area

Integration between new field observations with pre-existing data resulted in a new structural geological map of the Pajala region (Fig. 3). Geophysical lineaments, mostly derived from earlier geophysical studies (magnetics, VLF, slingram), were reinterpreted and grouped by orientation into four main groups: 1) N–S to NNE–SSW, 2) NE–SW, 3) NW–SE and NNW–SSE-striking lineaments. Observations on shear sense indicators and strike-dip measurements on strongly deformed rocks were

then linked to nearby geophysical lineaments. As a result, many lineaments displayed in Figure 3 could be “translated” into shear zones. Relative movements accommodated by these shear zones were derived from shear sense indicators or from displaced geophysical markers. Relative timing of shearing was determined for some shear zones based on the displacement or intersection by other shear zones. From this analysis we obtained the following sequence of shear zone activation: 1) Dextral shearing along N–S to NNE–SSW-orientated shear zones, 2) Dextral shearing along NE–SW-orientated shear zones, 3) Dextral shearing along NW–SE-orientated shear zones, 4) Sinistral reactivation along N–S to NNE–SSW-orientated shear zones.

The mapped folding pattern displayed in Figure 3 was derived from a combination of new and pre-existing strike-dip measurements of foliations and lineations (see stereographic plots). Magnetic anomaly maps were also used to determine the map trace of the fold hinges. The resulting pattern largely accords with earlier maps of the area (e.g. Bergman et al. 2001), but some more N–S and NW–SE-striking upright folds were recognised southeast of Pajala. Many of the folds in the Pajala region are aligned to shear zones, which may indicate a spatial and temporal relationship between the two structures. As such, the folds can be grouped according to the strike of axial planes into groups resembling the geophysical lineaments: 1) N–S, 2) NE–SW and 3) NW–SE-trending. With a subdivision of structural features based on orientation, two major deformation zones or belts can now be distinguished in the Pajala region: the Pajala deformation belt (PDB), in which shear zones, folds and main foliation predominantly strike N–S; and the Kolari shear zone, along which associated shear zones and folds strike mainly NE–SW. Both shear zones are shown on the structural geological map as large shear zones (belts) with a considerable width, i.e. tens of kilometres (Fig. 3). The Kolari shear zone clearly overprints the PDB, causing an eastward displacement of the PDB into Finland.

The migmatite domain

Folding patterns

The Migmatite domain is characterised by a predominantly N–S-orientated folding pattern. The scale of the observed folds varies from centimetres in outcrops to more than 4 km outlined by magnetic anomalies. Most mesoscopic folds observed in outcrops are upright folds with N–S-striking fold axes, and fold the main metamorphic fabrics (S1). Fold axes are typically shallow-plunging towards the south, but may also be doubly-plunging, producing dome shapes in outcrop and on a map scale. The absence of two intersecting foliations in outcrops suggests that the domes may not have resulted from fold interferences. However, superimposed folding as a dome-forming mechanism should not be excluded (see discussion in this chapter). On a map scale, many of the km-sized N–S-trending folds in the Migmatite domain appear as doubly-plunging folds resembling large dome geometries. The domes are ellipsoidal in an N–S direction and typically bounded by shear zones. Hinge zones characterised by shallow-dipping migmatitic fabric (S1) were observed in the core of some dome interiors (Fig. 4B). Apart from metamorphic banding, no axial plane cleavage was observed in these hinge zones. NW–SE-striking folds are generally obscured by N–S-striking folds and shear zones, and were only recognised in some outcrops (Fig. 4C). Directly east of Pajala, a series of folds with moderately southwest-dipping axial planes and sub-horizontally NE–SW-orientated fold axes strike parallel to the NW–SE-striking Kengis shear zone (Fig. 1, Fig. 4C). Like the N–S-striking folds, the NE–SW-striking folds clearly fold a migmatitic banding and should therefore post-date peak metamorphism.

Shear zones and tectonic lenses

The larger and dominant N–S-striking folds are typically bounded by 5–100 m wide shear zones characterised by low- to medium-grade protomylonites as well as pegmatites forming large vein networks. A simple shear component is often recorded together with predominantly dextral-slip indicators,

but sinistral slip was also observed (Fig. 4D–E). The shear zones acted as zones of weakness, along which progressive deformation was localised. Consequently, the folded domains embedded into the braided pattern of shear zones eventually behaved as tectonic lenses and were less affected by late ductile deformation.

The Koijuvaara shear zone

The Koijuvaara shear zone defines the western boundary of the PDB and is named after the type locality at Koijuvaara hill, southwest of Pajala. The shear zone includes the discrete Koijuvaara brittle-ductile shear zone, which stands out as a geophysical lineament (magnetics, VLF and slingram), as well as the higher-grade Koijuvaara mylonite zone, which extends 1 km east of the fault (Fig. 4).

The metasedimentary rocks along the Koijuvaara brittle-ductile shear zone contain a prominent N–S-striking spaced cleavage, along which bedding and metamorphic banding are folded (Fig. 4H). In the Koijuvaara area, primary bedding is well preserved inside the fold hinge and represents an alternation between quartz-feldspar layers and mica-rich layers. Mica-rich layers contain anhedral andalusite overgrown by euhedral staurolite. Biotite, muscovite and ilmenite inclusions in the staurolite are aligned, but not parallel to the main fabric, suggesting mineral growth between a first and second phase of deformation. The spaced cleavage usually strikes parallel to the axial planes of the minor folds, whereas in other cases it clearly crosscuts the folding pattern (Fig. 4G–J). Locally, these folds form ellipsoidal domes, typically with N–S to NW–SE-orientated axial traces (Fig. 4G). In addition, a fold interference pattern of N–S-orientated “heart-shapes” suggests multi-phase folding during NE–SW shortening and E–W shortening. To the south of Koijuvaara, horizontal dextral shearing overprinted by later sinistral shearing was inferred from microstructures, confirming Bergman et al. (2006), who described well-developed shear bands, indicating dextral movements in the Koijuvaara area. Metamorphic temperature and pressure were determined from a garnet-bearing sample by the same authors, recording up to 515 °C at 4.1 kbar.

Less than one kilometre east of Koijuvaara, paragneisses and mica schists are migmatitic and contain a penetrative, mainly N–S-striking, mylonitic fabric. The mylonitic foliation dips steeply eastward and strikes parallel to the migmatitic banding. Shear sense indicators, such as C–S fabric, imbricated clasts and mica-fish, are consistent with predominantly dextral shear, but sinistral shear was also observed. There are only a few observations on vertical sections, but they generally indicate eastern-side-up sense of shear. Moreover, quartz ribbons appear elongated, particularly in a vertical direction (L>S tectonite), suggesting that vertical movements were more intensive than strike-slip movement (Fig. 4M). The mylonitic fabric is best developed in biotite-rich paragneisses. Stratigraphic levels comprising layers of quartz-arenites are only weakly foliated and have preserved sedimentary structures. However, some local occurrences of weakly deformed quartz-arenites as boudins do indicate deformation. Another indicator of intense deformation in the mylonite zone is the strongly ellipsoidal outline of a large N–S-striking fold interpreted from the magnetic anomaly (Rasi syncline). Detailed studies and 3D modelling of the structure indicate that the fold is a steeply eastward-dipping, doubly-plunging syncline, which was probably formed by a combination of vertical shearing during NE–SW transpression and later flattening during E–W shortening (Luth et al. 2015, and section 5.5). The fact that the Rasi syncline is more elongated than the domes located further to the east suggests relatively high deformation in the Koijuvaara shear zone. In a few observations located around the fold hinge zone the mylonitic fabric appears folded, and the inferred mylonitic fabric is overprinted at an angle of 45 ° by a N–S-orientated spaced cleavage composed of unstrained micas (Figs. 4K–L). In most observations, however, the spaced cleavage strikes parallel to the mylonitic fabric and may be associated with brittle-ductile reactivation along the Koijuvaara shear zone.

Migmatite Domain

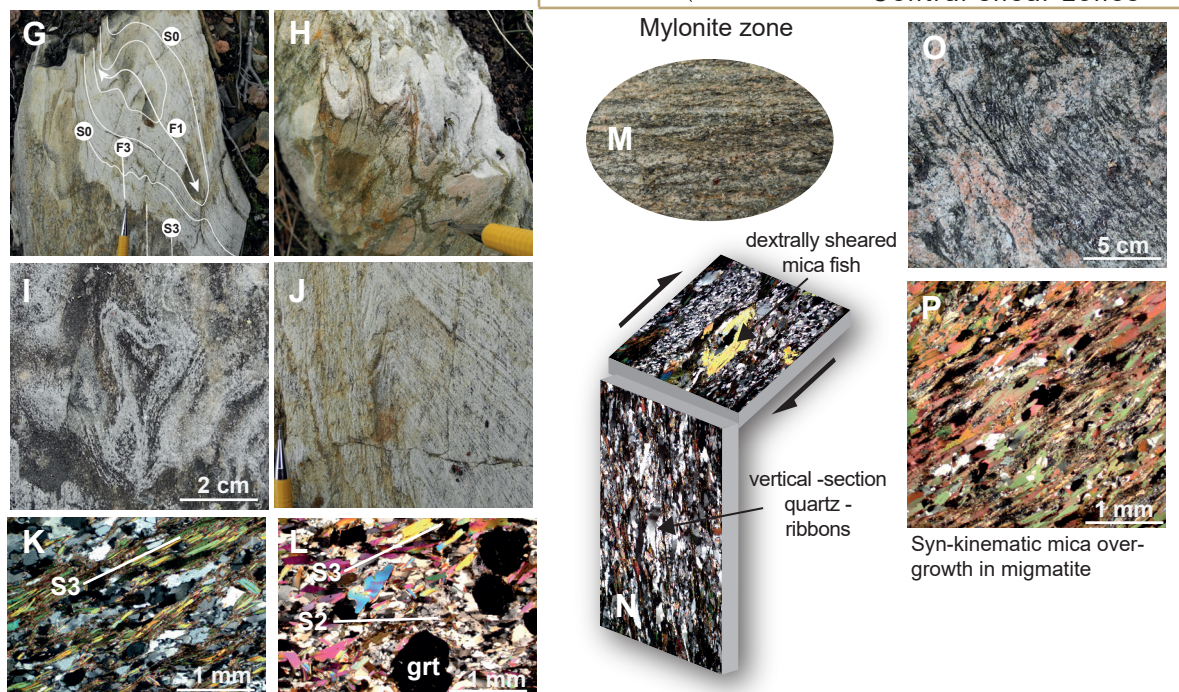
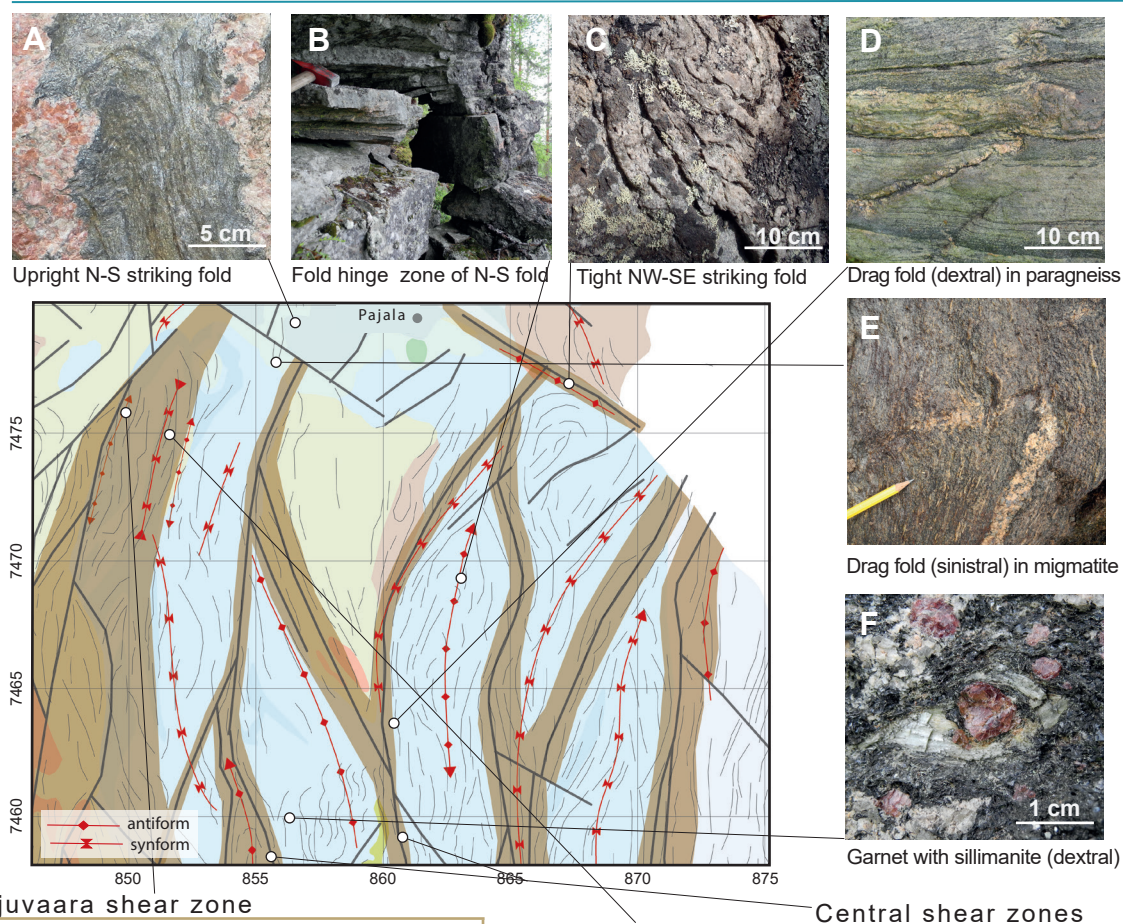


Figure 4. Observations and interpretations of structural features present in outcrops and thin sections from the Migmatite domain. Brown zones on the map indicate an estimated width of the major shear zones. For explanations of the other colours see legend in Figure 1.

Suorsa domain and Kolari shear zone

The Suorsa domain lies west of the Koiyuvaara shear zone and predominantly consists of weakly deformed intermediate volcanic and volcanoclastic rocks. Despite some alteration (scapolite, K-fsp, epidote), an andesitic composition was deduced from geochemical analyses (Luth et al. 2015). Deformation in the Suorsa domain is heterogeneous and mainly restricted to discrete NE–SW-striking ductile shear zones and faults. These deformation zones are interpreted from lineaments derived from magnetic and VLF anomaly maps (Figs. 2, 5 and 6). It is clear from the apparent resistivity map that the NE–SW-striking lineaments crosscut the N–S-striking lineaments associated with the Koiyuvaara shear zone further east. Geological observations along some of the NE–SW-striking lineaments reveal altered mylonites as well as strongly deformed fault rocks (Fig. 5A–E). Kinematic indicators in the mylonites are mostly consistent with dextral strike-slip (Fig. 5), but sinistral strike-slip has also been observed. Typically, a few tens of metres away from the deformation zones, the rocks are only weakly deformed and often lack foliation or metamorphic banding (Fig. 5F–G). Consequently, the NE–SW-striking lineaments should be treated as narrow, localised deformation zones. Based primarily on their orientation and continuation towards the northeast (Finland), we consider the deformation zones to represent the southwestern segment of the Kolari shear zone (see also Figs. 1, 3 and discussion). In addition, subsurface geometries of the zones were obtained from 2D resistivity models based on new VLF data (Fig. 6). The resulting models reveal sub-vertically dipping deformation zones corresponding to low-resistivity domains (Fig. 6). Along strike the low-resistivity domain widens towards the NE from 300 m to 1 km (see sections 1 and 7). This transition from a narrow to a wider system coincides with the intersection between the Kolari shear zone and the Koiyuvaara shear zone. The exact dip of the deformation zones remains difficult to interpret from the modelling results; however, a steeply eastward dip can be deduced from some sections (e.g. 1, 5 and 8).

Local deformation in the Suorsa domain

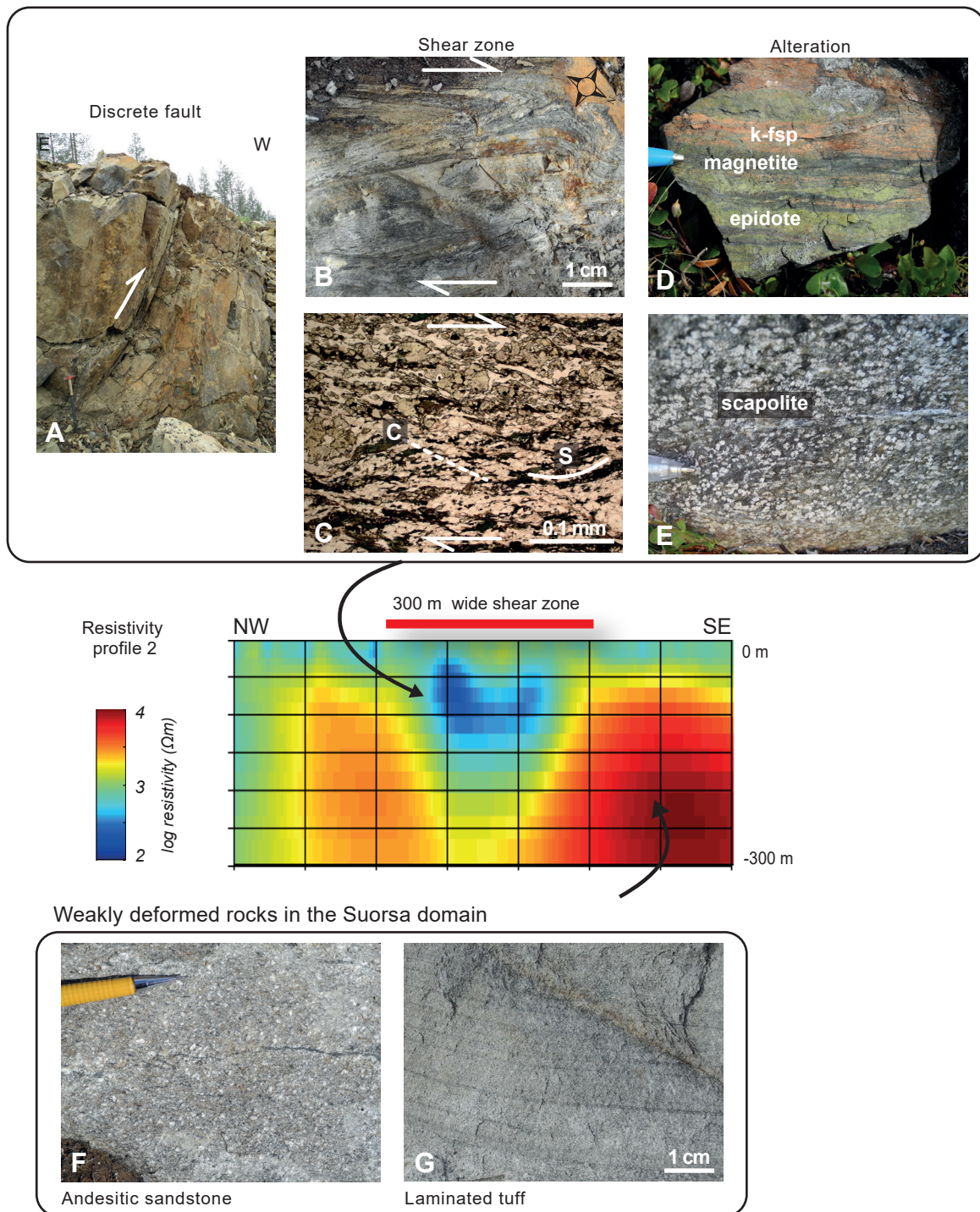
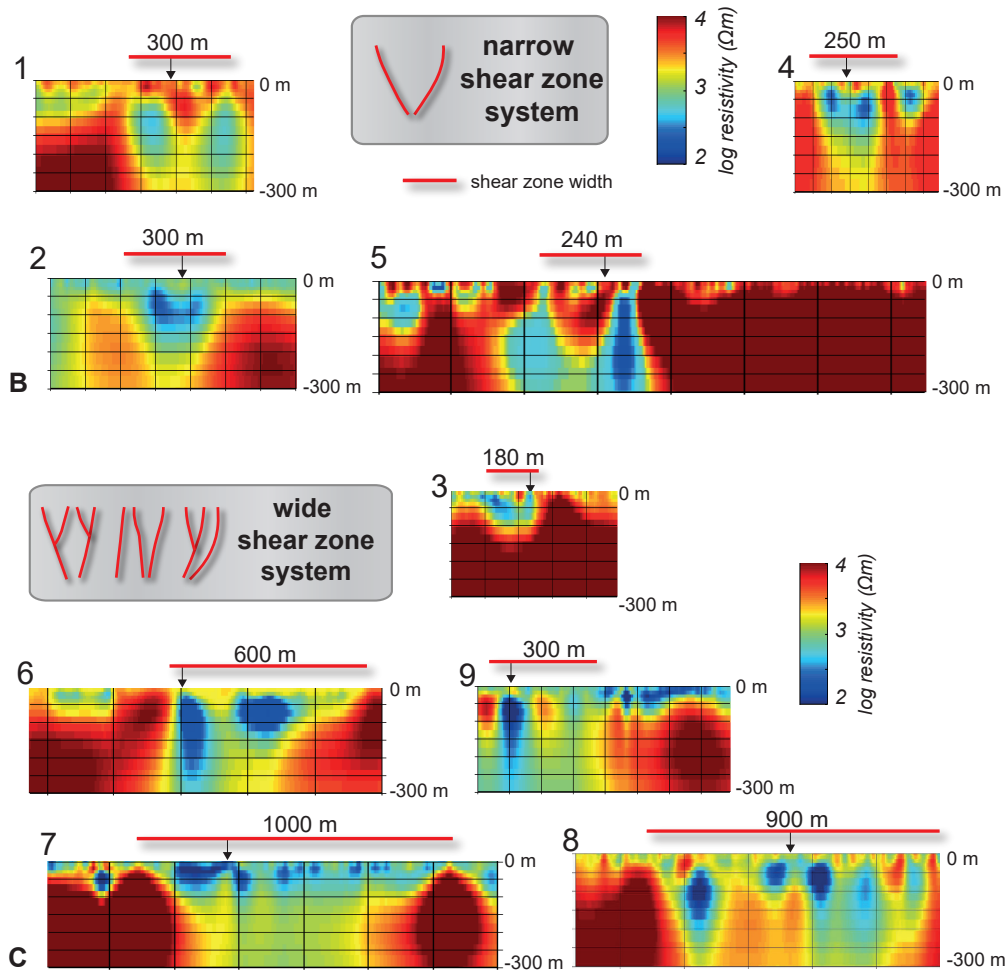
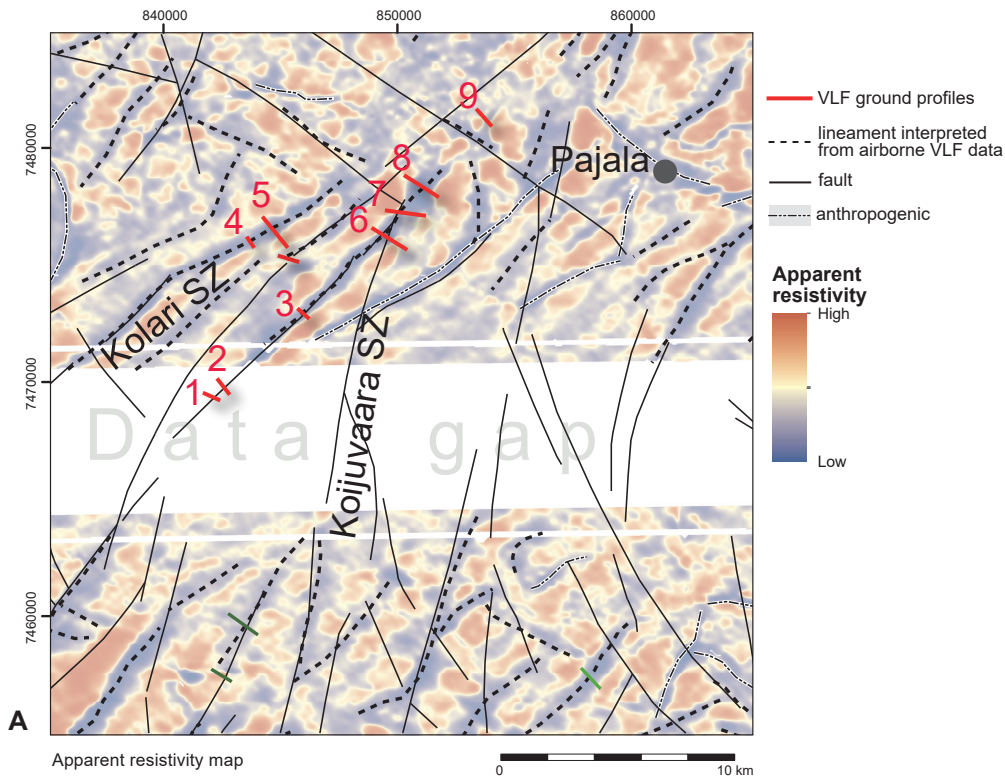


Figure 5. Examples of deformation in the Suorsa domain. Discrete faults and shear zones with associated potassium alteration and mineralisation (iron-oxides and sulphides) (A–E). The zones separate areas of weakly deformed rocks, with primary textures often well preserved (F–G). The resistivity profile, derived from ground measurements of electromagnetics, defines the shear zones as domains of low resistivity. Location of profile 2 is shown in Figure 6.

► Figure 6. Resistivity 2D models of the Koijuvaara and Kolari shear zones based on data from electromagnetic ground measurements. A. VLF anomaly map with locations of numbered profiles as red lines. B–C. Profiles of resistivity 2D models. The results can be grouped according to the width and geometry of the interpreted faults or shear zones into a “wide shear zone system” and a “narrow shear zone system”. Note that the wider system coincides with the region of intersection between the Koijuvaara shear zone and the Kolari shear zone. The black arrow points to the shear zone in map view.



2D REGIONAL GEOPHYSICAL MODELLING AND GEOLOGICAL INTERPRETATION

2D forward modelling of gravity and magnetic data along a WNW-ESE-striking profile (Fig. 2) allowed for a better constraint on the geometry of the major boundaries within the PDB at depth. Petrophysical parameters from samples combined with in situ measurements of magnetic susceptibility along the profile were acquired to constrain the model. The subsurface geometries obtained are interpreted geologically as a large crustal wedge-shape bounded by steeply opposing dipping shear zones (Fig. 7). The Koijuvaara shear zone is modelled as a steeply eastward-dipping shear zone. Shear zones in the central part of the PDB dip sub-vertically towards the west. Also the Kolari shear zone in the Suorsa domain appears as a narrow crustal wedge with steeply opposing dipping shear zones.

Construction of the 2D geophysical model

Tonalitic-granodioritic rock occurs in the western part of the profile and is visualised as the brown body in Figure 7. 22 petrophysical samples were acquired from this lithology, yielding an average density of 2.73 g/cm^3 . The median magnetic susceptibility of these samples is $3\,000 \times 10^{-5}$ SI units. East of the tonalite-granodiorite a granite outcrops at the surface (red in Fig. 7) and was sampled at 14 locations. Its average density is 2.63 g/cm^3 and its modelled depth extent is approximately 1 500 m below the surface. The granite has a relatively low content of magnetic minerals, resulting in an average susceptibility of 500×10^{-5} SI units. There are some strong positive magnetic anomalies within the granite caused by dolerites. The dolerites have been sampled at one location; the density for that sample is 3.11 g/cm^3 . The content of magnetic minerals is quite high in the dolerite, with a susceptibility of almost $50\,000 \times 10^{-5}$ SI units. The in situ measurements with a susceptibility meter on the dolerite give an average value of $29\,000 \times 10^{-5}$ SI units. The bodies in the model that represent the dolerite (shallow purple bodies in Fig. 7) have therefore been assigned a magnetisation value of $40\,000 \times 10^{-5}$ SI units. This corresponds fairly well with the observed data and also indicates that the dolerites dip to the northwest. There is a sharp, positive gravity anomaly east of the granite, corresponding to intermediate volcanic rock (light green in Fig. 7). Seven petrophysical samples from this lithology give an average density of 2.8 g/cm^3 . In situ measurements of magnetic susceptibility on outcrops give an average value of $4\,000 \times 10^{-5}$ SI units. The modelled depth extent of the volcanic rock is around 2 000 m below ground surface and is wedged between the intrusions in the west and the sedimentary rock in the east.

A meta-arenitic rock borders the intermediate volcanic rocks to the east (light blue in Fig. 7). It is seen in the geophysical data as a low-magnetic and low-gravity area, which accords well with the petrophysical samples analysed from this lithology. Three petrophysical samples give an average density of 2.63 g/cm^3 , and a very small quantity of magnetic minerals yield a susceptibility of around 10×10^{-5} SI units. According to the observed magnetic field, however, there are some high magnetic anomalies within the meta-arenite, although these have not been taken into account in the model. The meta-arenite is bordered to the east by a thin sliver of granite (red in Fig. 7), which is considerably more magnetised than the metasedimentary rock. Five petrophysical samples of the granite have been collected roughly seven km south of the profile. The average density is 2.65 g/cm^3 . In situ measurements of magnetic susceptibility on outcrops give a median value of $7\,000 \times 10^{-5}$ SI units. Taken together, the magnetic and gravity data indicate that the contact between the granite and the metasedimentary rock dips fairly steeply. The relatively high magnetic field continues further east, where the gravity field is also high. This corresponds to the intermediate metavolcanic rock (light green in Fig. 7). However, no petrophysical samples have been collected from this lithology close to the profile, so the modelled body has been given the same physical properties as the intermediate metavolcanic rock further to the west, i.e. 2.8 g/cm^3 and $4\,000 \times 10^{-5}$ SI units for the density and magnetic susceptibility, respectively. A large area of paragneiss occurs east of the metavolcanic rock, visualised as a light blue body in Figure 7. The magnetic field is relatively heterogeneous and the gravity field is quite high. In the vicinity of the pro-

file, within 5 km on both sides, 13 petrophysical samples have an average density of 2.80 g/cm^3 and a median magnetic susceptibility of $6\,000 \times 10^{-5} \text{ SI}$ units. The heterogeneity in the magnetic field has not been addressed in this model. The main geometry of the paragneiss is the dip to northwest and the thinning out at depth to the southeast. An area of considerably higher magnetisation occurs within the paragneiss close to the southeastern boundary with the granite. There are no ground observations in this magnetised lithology, however, so it has been assigned the same density as the surrounding paragneiss (2.80 g/cm^3), but with a higher magnetic susceptibility of $11\,000 \times 10^{-5} \text{ SI}$ units. It is seen in Figure 7 as a darker blue body. The profile ends in the southeast in a granitic rock (red in Fig. 7). Three petrophysical samples have been collected from this granite within less than 1 km from the profile. The average density is 2.61 g/cm^3 , and a relatively moderate magnetic susceptibility of approximately $1\,000 \times 10^{-5} \text{ SI}$ units was obtained. The gravity field over the granite and the adjacent paragneiss indicates that the granite dips under the more dense metasedimentary rock.

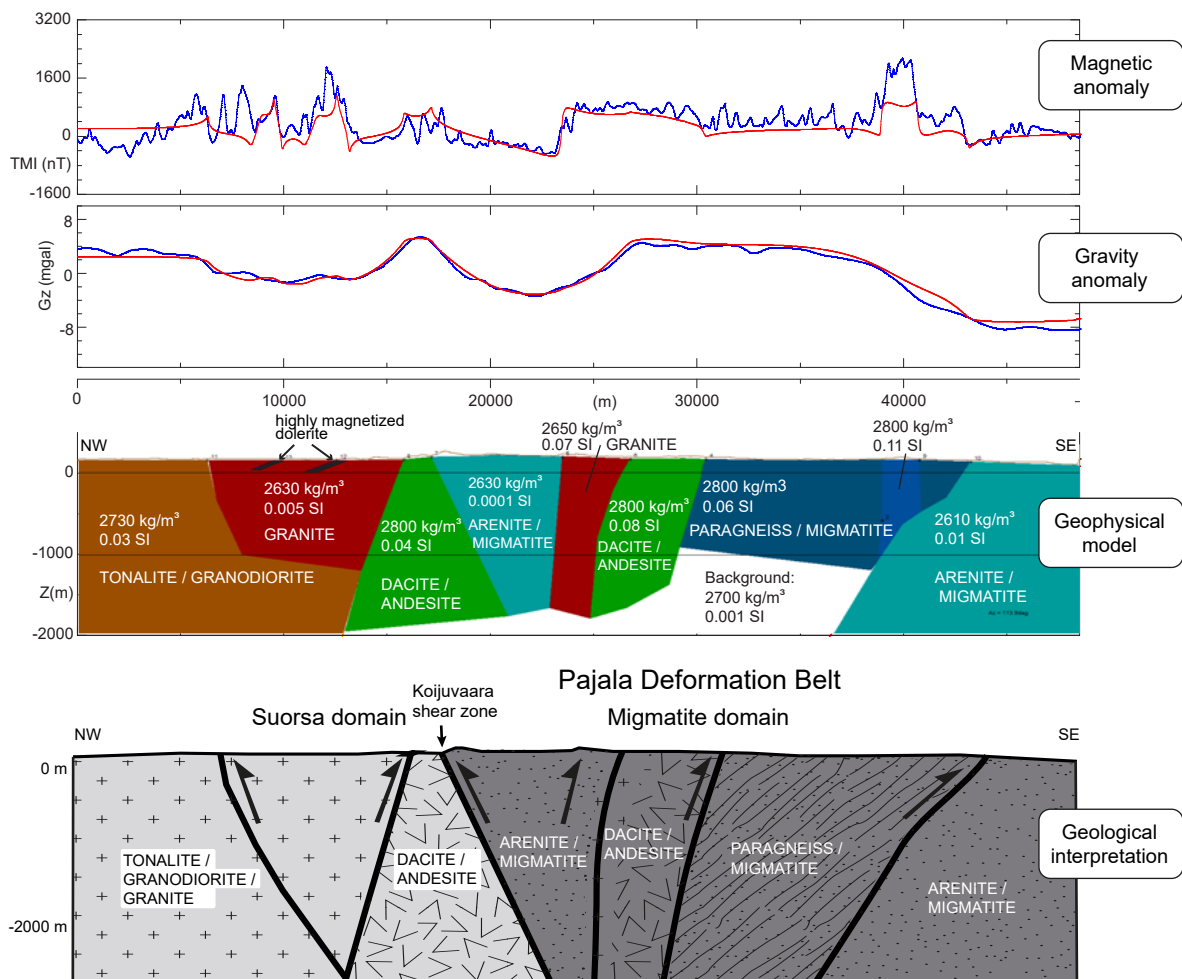


Figure 7. 2D geophysical model and geological interpretation of the PDB (profile location is shown in Figs. 2A–B). The model (bottom view) is based on airborne magnetic (top view) and gravity data (middle view). Blue and red lines represent the measured and calculated values, respectively. See text for more detailed explanations.

LOCAL AND SEMI-REGIONAL 3D MODELS

Input data and methodology

Local and semi-regional 3D models were constructed primarily to constrain subsurface geometries of structural features shown on the geological and geophysical anomaly maps (Figs. 2, 3). The resulting 3D geometries provided the framework for the conceptual regional-scale model presented in section 6.2 (Fig. 12). Input data for the local 3D models were geological field observations and structural measurements, geophysical potential field data and, for the Liviövaara model, drill core data as well. Geophysical potential field data were processed using Geosoft, Voxi and ModelVision modelling software packages. These modelling results were then compiled and visualised in combination with geological data using Gocad Paradigm.

Eastern folds model

The Eastern folds model is located in the east of the Migmatite domain (Fig. 8). Its dimensions are approximately 9 km east–west by 18 km north–south. The model was selected to resolve the subsurface geometry of a series of N–S-striking folds. The model reaches down to 4 km, but the depth extent of the interpreted bodies does not exceed 2 km. The cell size of each volume pixel (voxel) in the model is 100 × 100 m laterally and 50 m vertically. Before the data were inverted, voxels were assigned minimum and maximum magnetic susceptibility constraints. These constraints were provided by available petrophysical data from the area, along with in situ susceptibility measurements on outcrops. Based on a total of 42 petrophysical samples, the constraints on the model have been set within 0 and 0.2 SI units. The grid obtained was then imported into Gocad, where N–S and E–W-orientated sections were extracted from the grid volume. Each section was then interpreted manually, focusing primarily on the large-scale folding pattern. An interpolation between the sections was made, resulting in an undulating surface that reflects the overall 3D folding style within the domes.

A remarkable result from the Eastern folds model is an internal structure characterised by multiple aligned “domes and basins”. As such, relatively long wavelength folds are interpreted from the N–S-orientated section, whereas folding is tight in the E–W-orientated sections. In addition, section 1 reveals a pattern of steeply west-dipping folds, bounded and intersected by moderately west-dipping zones. The combination of observations on sense of shear in outcrops and the geometry deduced from the geophysical models implies tectonic transportation was directed to the east in this part of the Pajala deformation belt.

Central model

The model area measures 9 by 16 km and is located in the centre of the Migmatite domain. The lithology of the selected area was mapped as intermediate metavolcanic rocks, but this interpretation is based on only a few field observations. Contrastingly, new field observations made for the present study reveal a gneissic to metagranodioritic lithology. It may be assumed that the coinciding relatively high magnetic and gravity responses may actually have a deeper source. The model depth is 2 km and the cell size of each volume pixel (voxel) in the model is 100 × 100 m laterally and 50 m vertically. Before the data were inverted, voxels were assigned minimum and maximum values ranging between 0 and 0.15 SI units for magnetic susceptibility constrained by petrophysical data. N–S and E–W-orientated sections were extracted from the resulting grid volume. Interpretation of and interpolation between the sections resulted in an undulating surface representing the base of the high anomaly body. In addition, a high anomaly body with a relatively high magnetic susceptibility was constrained by isosurfaces.

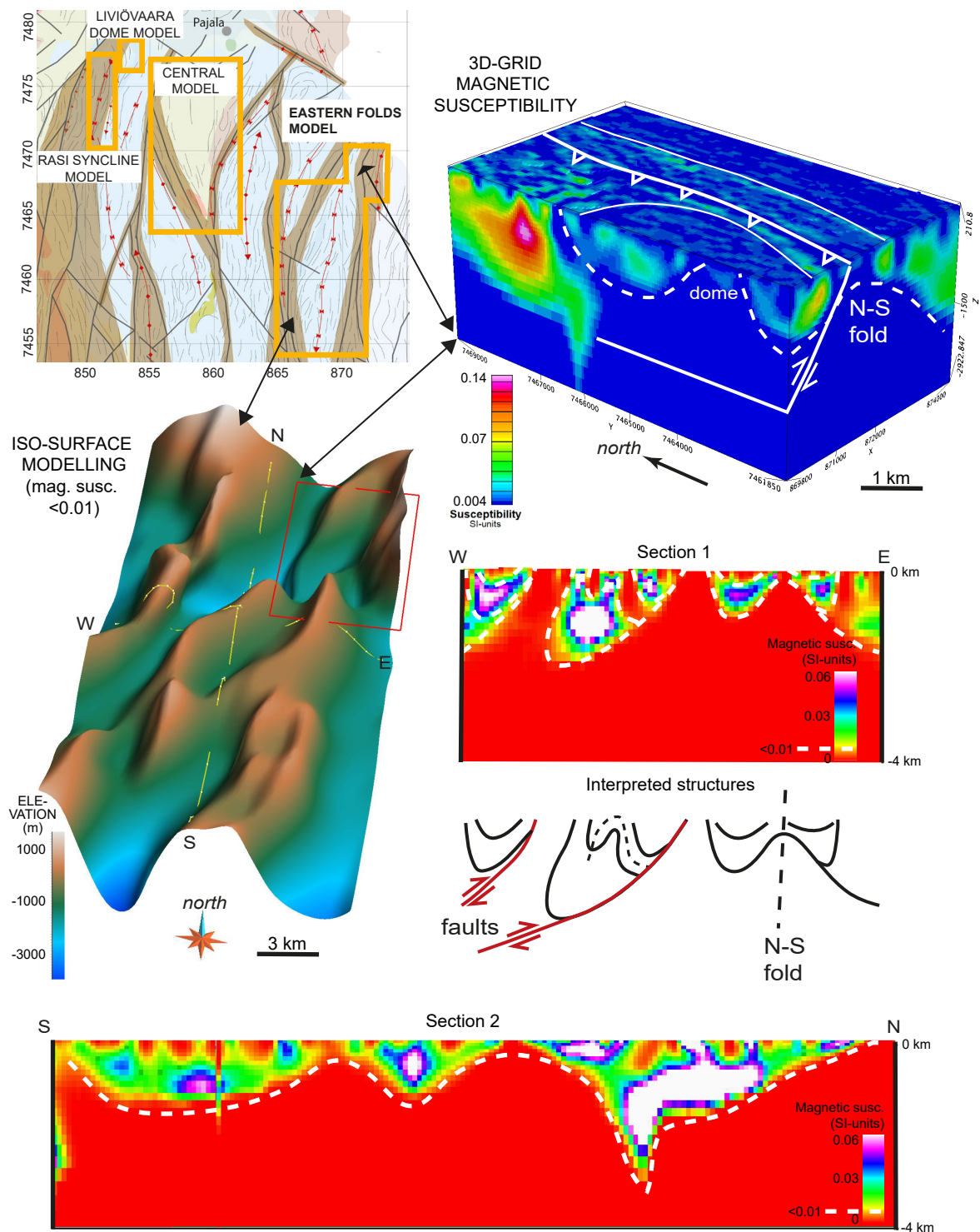


Figure 8. 3D model and interpreted cross-sections of the Eastern folds (see map insert for location). Several folds associated with shear zones are interpreted from the 3D magnetic susceptibility model (upper right). The undulating surface represents the lower limits of magnetic susceptibility and was extracted from the 3D model (middle left). Two sections through the model with an interpreted folding pattern are displayed to the right and below.

The resulting 3D model reveals a high-magnetic planar body underlying the area at a depth between 500 and 2000 m (Fig. 9). The body is heart-shaped and dips moderately towards the south. The body appears to be folded in a similar style to the “Eastern dome model”, with long wavelength, relatively open E–W folds and shorter-wavelength folds striking N–S. Whereas only low magnetic rocks were found at the surface, the modelled body may explain the region’s relatively high and constant magnetic anomaly. The rock type of the modelled high magnetic anomaly body remains unknown. However, the relatively high gravity anomaly in the area may be consistent with gabbro or basalt.

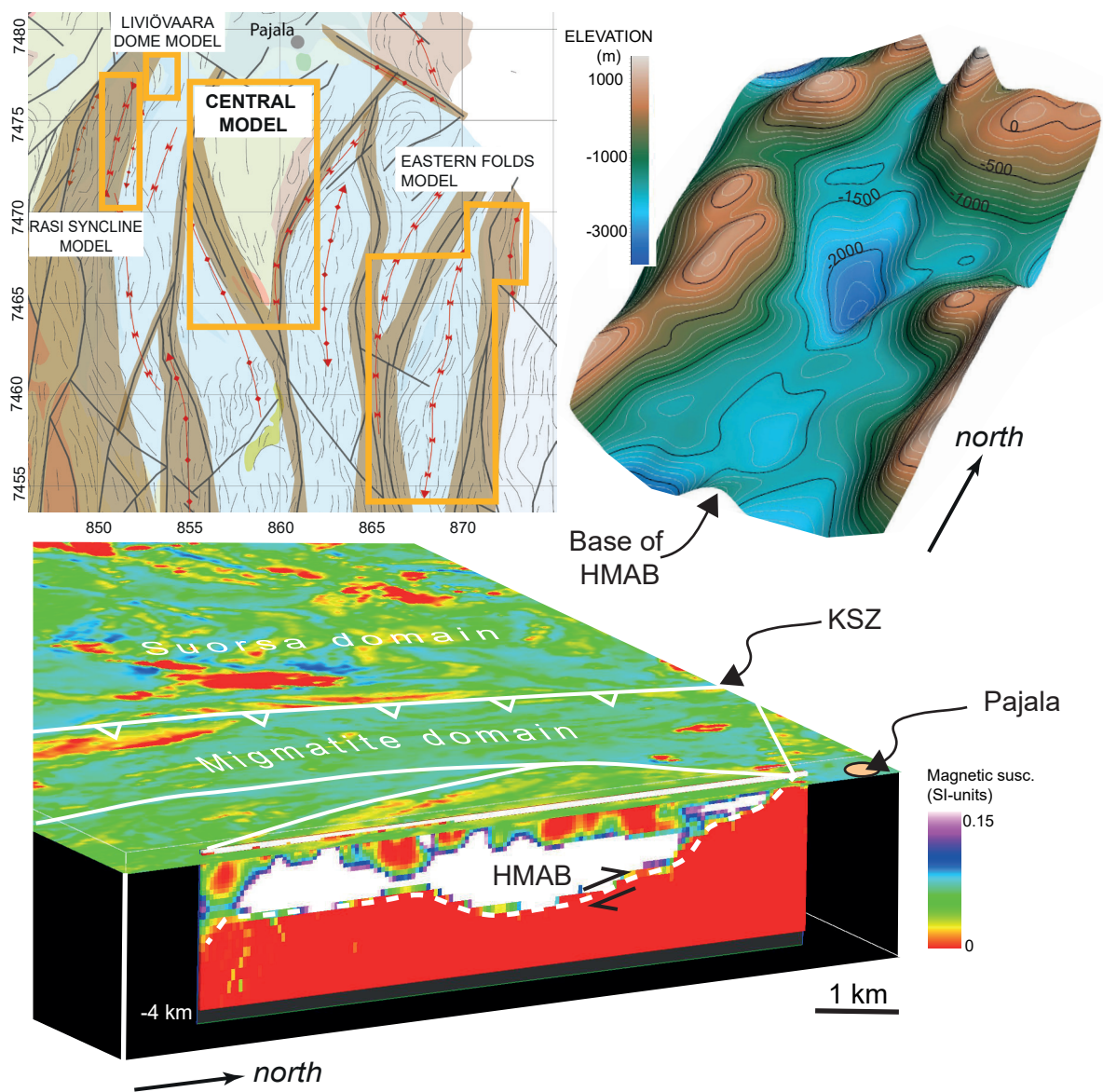


Figure 9. 3D local model of the central part of the Migmatite domain. A large tabular body with high magnetic susceptibility (HMAB) is hidden directly below the surface (magnetic anomaly map). The broken white line is the interpreted lower base of the body (lower view). The surface created in Gocad represents the lower base of the tabular body (upper view).

Liviövaara dome model

This model is mainly constrained by ground magnetic data, slingram and drill core data (see also Johansson 1985). No outcrops were located in the modelled area, which measures only 2 by 2 km (Fig. 10). Drill core data have shown that the area is underlain by metasedimentary and metavolcanic rocks, and also by gabbroic and monzonitic intrusive rocks. Some drill cores contained graphite schist and several limestone horizons were drilled, some of which were ore-bearing (Gerdin et al. 1990). Three

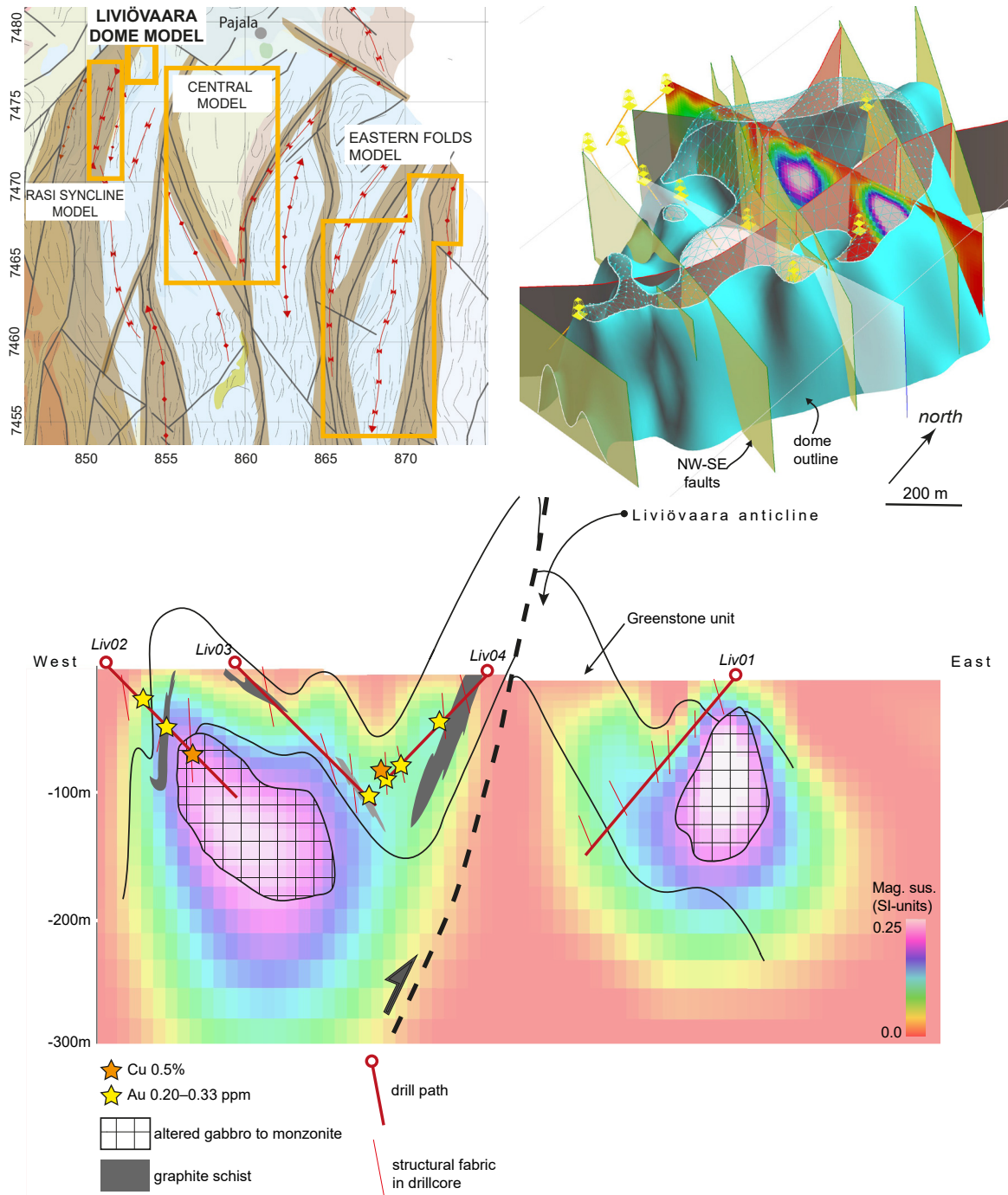


Figure 10. 3D local model of the Liviövaara dome (upper right). Interpreted cross-section through the dome, based on magnetic inversion modelling results and drill core data, is shown in the lower view.

types of ore were identified: 1) Cu-Au in altered rhyolites; 2) Cu-Au in altered limestone; and 3) Cu-(Ni-Au) in intrusive rocks (Gerdin et al. 1990).

The purpose of this model is twofold: to visualise in high-resolution local folding and faulting patterns in 3D, and to relate drill core data to the modelling results based on geophysical data. The model was constructed by the following steps: 1) Unconstrained inversion of ground magnetic data using VOXI. The cell size of each volume pixel (voxel) in the model is 10×10 m laterally and 5 m vertically; 2) import of inversion results, Lidar, drill holes, geophysical maps (ground magnetics and slin-gram) and lineaments into Gocad; 3) digitising of fault and fold outlines; 4) Creation of iso-surfaces surrounding domains with equal values for magnetic susceptibility derived from the inversion; 5) creation of a fault network constrained by map traces and iso-surfaces; and 6) interpretation of folding pattern based on magnetic inversion and drill core data.

The 3D model reveals a large antiformal dome, including several smaller sub-domes (Fig. 10). A NNE–SSW-striking deformation zone dipping steeply towards the west curves into the modelled area and offsets the antiform in a reverse sense. This deformation zone is displaced dextrally by a series of steeply dipping NW–SE-striking faults, which also accommodate a vertical slip component inferred from staircase stepping of the dome’s map trace. Both the northern and southern boundaries of the dome are abrupt due to this late faulting. The high-magnetic bodies located on both fold limbs correlate with intrusive rocks, which were drilled only on the dome’s western limb. The structural fabrics derived from drill cores consistently dip steeply to the east, which, together with the asymmetric parasitic fold located on the western limb, may suggest westward tectonic transportation.

Rasi syncline model

In the westernmost part of the PDB an elongated fold structure has been outlined (Fig. 11) and its deeper geometry investigated (see also Luth et al. 2015). Additional measurements have been carried out, and a refined model of the northern part of the fold is presented below, based primarily on new ground magnetic measurements. The total length of acquired ground magnetic measurements is approximately 20.5 km. In areas where ground measurements were lacking the model is based on magnetic anomaly data from airborne measurements, with a line separation of 200 m and point distance of approximately 35 m. A forward modelling procedure has been used. Other available data restricting the parameters have been used to limit the degree of freedom in creating the bodies. These data include structural measurements and laboratory measurement of the magnetic susceptibility and remnant magnetisation. In general, the bodies have a simple tabular geometry, assumed to represent elevated magnetic susceptibility layers embedded into a sequence of metasedimentary rocks. All bodies have been assigned an approximate depth extent of 500 m. For the sake of simplicity, the surrounding rocks are set to have a magnetic susceptibility value of zero. Physical properties of two samples collected from the magnetic layer were used to set further boundary conditions for the model (Fig. 11). In general, the magnetic horizons consist of two layers of higher magnetite content, but one and three layers are also observed in the data. The width of these layers varies between 4 and 40 m.

The resulting subsurface geometries of the strongly ellipsoidal Rasi syncline are shown in Figure 11. The fold appears entirely closed with the fold axis dipping towards the centre of the structure. In the northern half of the model, both folds limbs dip steeply to the east, whereas in the southern half the eastern limb dips steeply inwards to the west. The latter implies that the fold should be considered a doubly-plunging syncline, which is consistent with geological observations of cross-bedding, indicating stratigraphically younger rocks towards the centre of the fold.

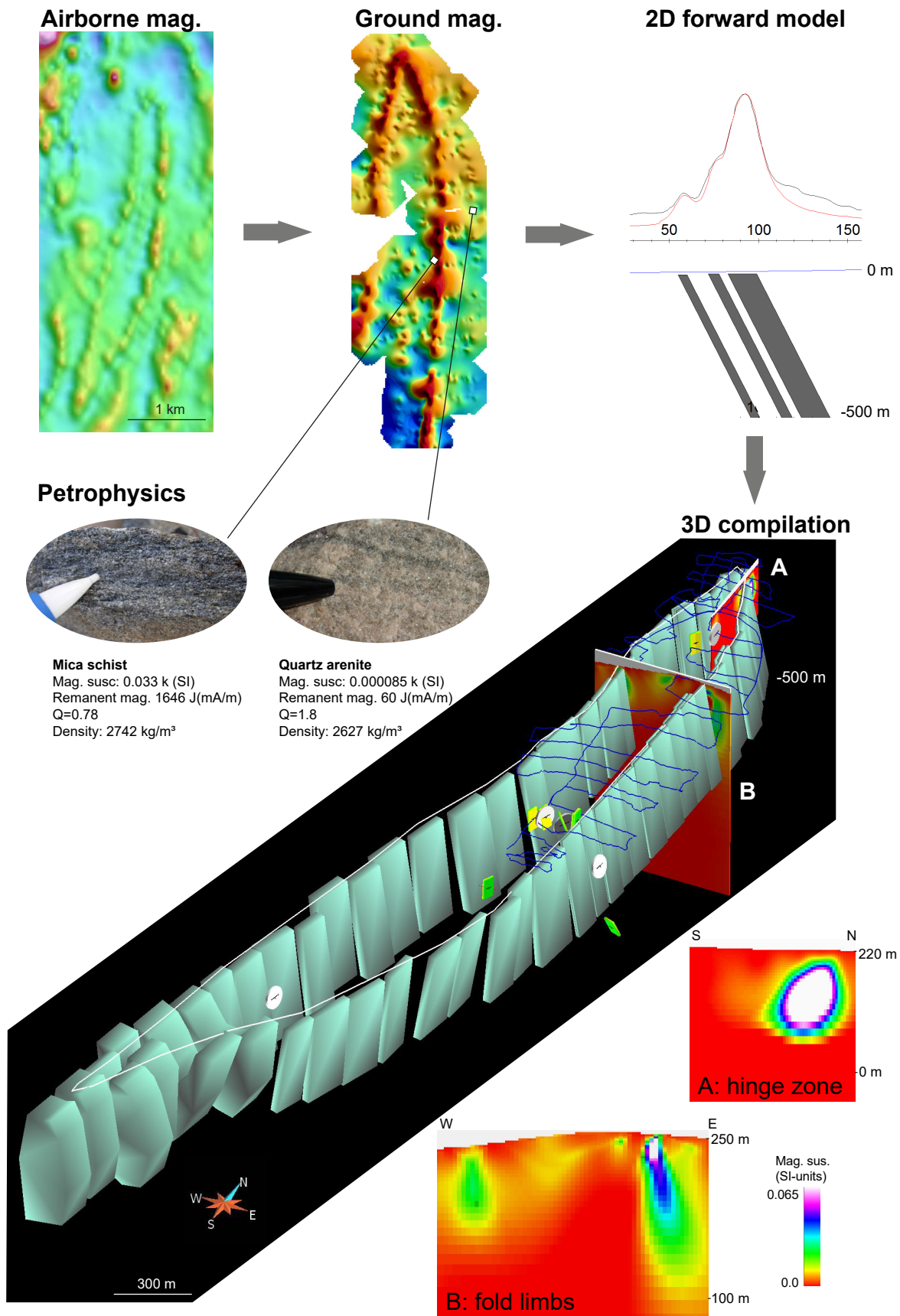


Figure 11. Construction chart of the 3D model of the Rasi syncline (see map insert in Fig. 10 for location). A combination of new ground magnetic data, sampling for physical rock properties and geological mapping was used to constrain the subsurface outline of the syncline.

DISCUSSION

On the origin of folds and domes

Earlier studies in the Pajala area postulated that major northwest–southeast-trending folds (F1) became refolded along north–south-trending F2 folds (Eriksson 1954, Padget 1977; see also Grigull et al., 2018). Following their interpretations, some of the smaller and larger dome patterns observed within the PDB in this study can be explained as the result of interference between NW–SE-orientated F1 folds and N–S-orientated F2 folds. Examples of some large-scale superimposed folds within the PDB may be represented by the modelled undulating surfaces underlying the eastern fold (see previous section and Fig. 8). In outcrop, superimposed folds were clearly observed along the Koijuvaara shear zone, marking the western border of the PDB (Fig. 4). In addition, heart-shaped patterns outlined on various scales (outcrop and 3D modelled surfaces) may also be considered the expression of F2 refolding F1. As such, the F1 axial planes may initially have dipped moderately to the southwest, whereas the superimposed F2 folds were more upright.

Another mechanism that could have produced the observed dome geometries, or “doubly-plunging-folds”, within the PDB is vertical shearing or extrusion. Vertical extrusion is the upward flow of material, and can be promoted by intensive shortening of rock units bounded by more competent units along steeply dipping boundaries. Most of the domes and larger folds within the PDB are indeed associated with steeply dipping shear zones, which often form the contact between domains of intensively folded migmatite and domains of more massive, weakly deformed intrusive or volcanic rocks (Fig. 12). In addition, a predominant component of vertical shearing is inferred from shear indicators observed in outcrops and thin sections (Fig. 4). An important tectonic implication of assigning a role to vertical extrusion is that the domes observed within the PDB can be explained by a single shortening event and therefore may not necessarily be considered the result of F1-F2 fold interference.

4D tectonic evolution of the Pajala region

Based on new observations and insights obtained from the modelling results, we propose three distinct phases of shortening that explain most of the structural features observed within the PDB and its immediate surroundings (Fig. 13). Most of these structures, including the predominant foliation and metamorphic banding, formed as a result of NE–SW transpressive bulk shortening (D1). During this stage the PDB evolved into a N–S-striking transpressional ductile wedge bounded by major shear zones, such as the Koijuvaara shear zone to the west (Fig. 12). Shearing along the N–S-orientated shear zones was oblique, or may also have been partitioned into vertical and dextral components among the different shear zones. The folding pattern observed between the shear zones of the PDB most likely formed during D1 NE–SW transpressive bulk shortening. As such, NW–SE-trending folds (previously considered F1 by Eriksson (1954) and Padget (1977)), as well as N–S-orientated folds (previously considered F2) may both have resulted from strain partitioning operating on several scales. It has been shown by Tikoff and Peterson (1998), among others, that in transpression, folds may form obliquely to the tectonic transport direction at an angle of 40–50°. In addition, rotation caused by non-coaxial strain within the PDB could have rotated some of the earlier formed NW–SE-trending folds into a N–S orientation (Figs. 12 and 13). With ongoing NE–SW transpression, the PDB may have finally reached a kinematic stage of full-strain partitioning between strike-slip in the central part (Migmatite domain) and reverse displacements, with folding and thrusting along the margins (Koijuvaara shear zone). This stage is the final distinct kinematic stage observed in analogue experiments on transpressive wedges presented by Leever et al. (2011). Large vertical displacement along steeply dipping major shear zones promoted vertical extrusion and the formation of several domes and doubly-plunging folds adjacent to the shear zones. With ongoing shortening and exhumation of the wedge, deformation became more localised along discrete shear zones, and NE–SW-striking Riedel shears were likely to form. In analogue experiments where the shortening direction is at an angle of

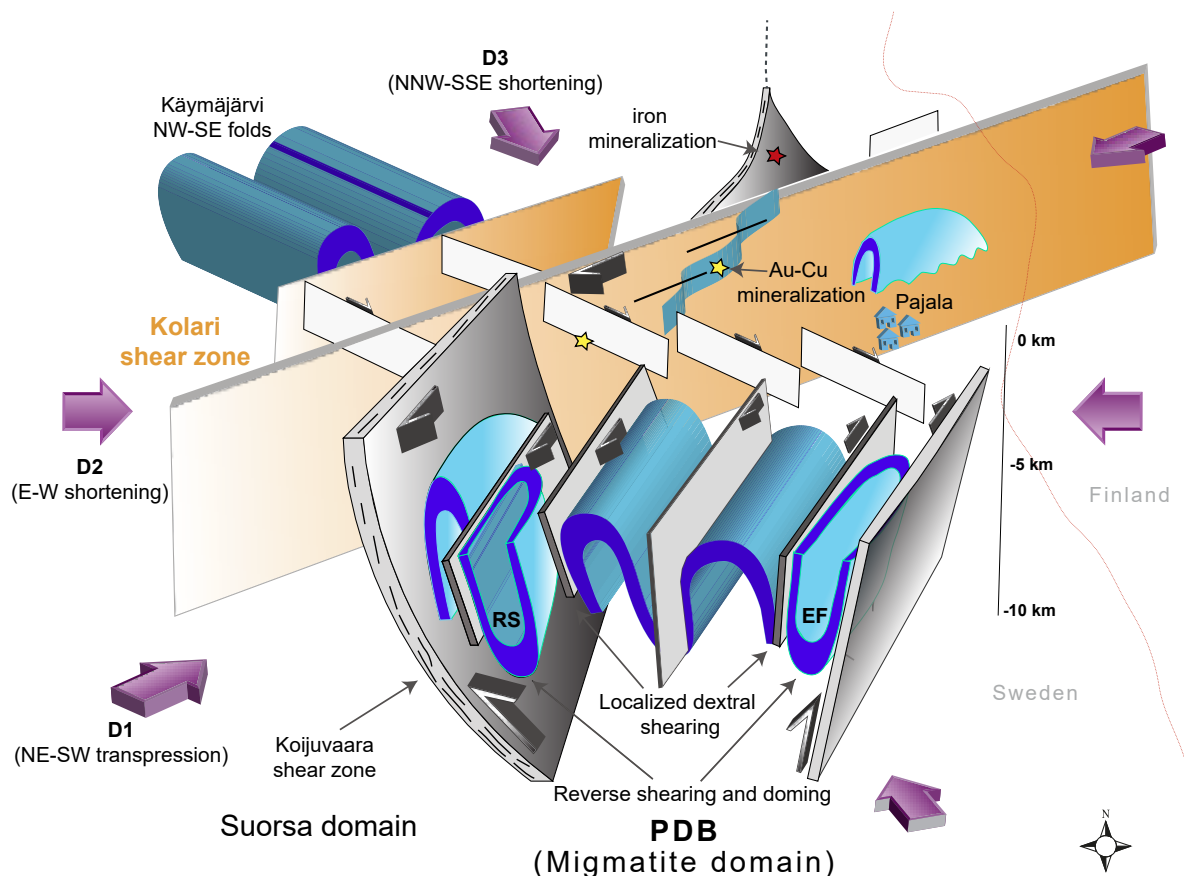
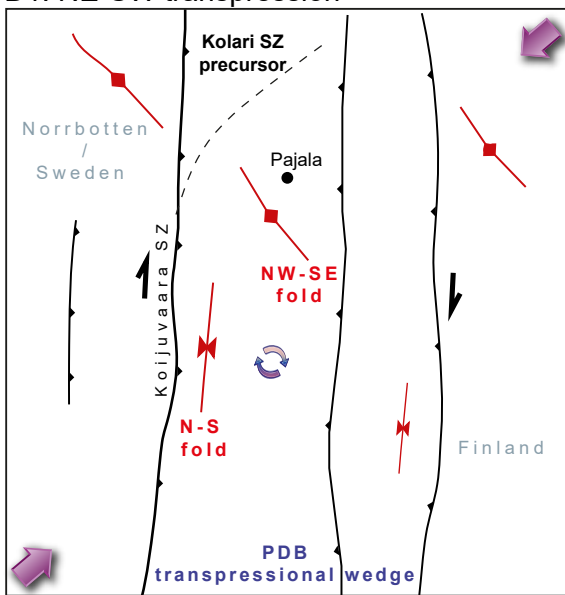


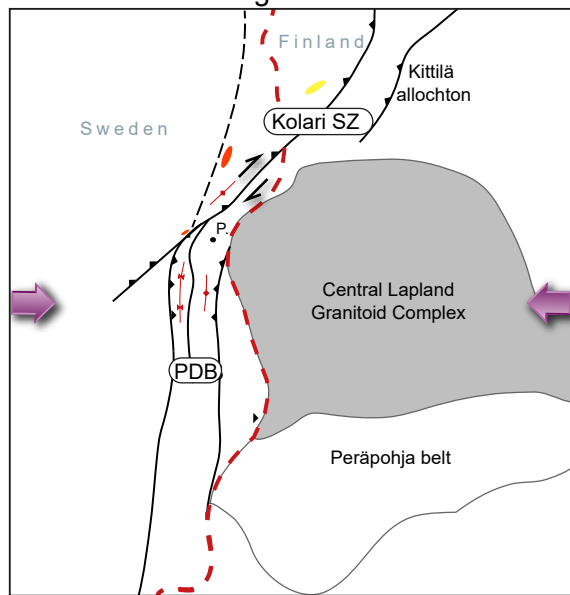
Figure 12. 3D conceptual model of the Pajala deformation belt (PDB) and the Kolari shear zone in the Pajala area (not to scale). The PDB is represented by a transpressional wedge outlined by major shear zones accommodating both vertical and dextral movements. Within the wedge, strain partitioning during D1 NE–SW shortening resulted in upright, cylindrical and non-cylindrical, N–S-trending folds, which became intersected by parallel striking, mainly dextral, shear zones. North of Pajala, the wedge is disrupted by the NE–SW-striking Kolari shear zone as well as by a set of en-echelon W–NW–E–SE-orientated faults and shear zones, formed during D2 E–W and D3 N–NW–S–SE crustal shortening, respectively (see also Fig.13). RS: Rasi syncline (Fig. 11), EF: Eastern folds (Fig. 8). Purple arrows indicate direction of regional shortening. The thin red line marks the national border between Sweden and Finland.

15° to the plate boundary, NE–SW-striking structures formed, mimicking the orientation of the shear zones observed in the Suorsa domain. It is therefore very possible that a precursor of the Kolari shear zone had already formed at this stage. The Kolari shear zone did not, however, develop into a major shear zone accommodating dextral displacements before stage D2 (E–W shortening), which finally resulted in an eastward offset of the entire PDB north of Pajala. Consequently, the Kolari shear zone should be treated as a separate shear zone system, rather than part of the PDB, as was proposed in earlier studies (e.g. Niiranen 2011). We suggest that during D2 E–W shortening the central Lapland granitoid complex located directly east of the PDB acted as a large rigid unit, along which deformation in the surrounding supracrustal rocks became localised, and structural features were reshaped towards parallelism along its contact (Fig. 13). E–W shortening was then primarily accommodated by reverse shearing, fold amplification and flattening. The larger folds eventually evolved into tectonic lenses, and deformation became localised along the limbs. A relatively high elongation (length/width ratio = 9/1) of the Rasi doubly-plunging fold may indicate that E–W flattening was most severe along the PDB’s western border (Koijuvaara shear zone). Deformation finally became brittle during the last shortening stage D3 (N–NW–S–SE shortening). Conjugate faults, of which the WNW–ESE-orientated dextral faults are often the best developed, crosscut all other fabrics observed within and outside the PDB. At some localities, such as Liviövaara, the individual faults also accommodate tens of metres of vertical displacements, as inferred from a few brittle-ductile kinematic indicators.

D1: NE-SW transpression



D2: E-W shortening



D3: NNW-SSE shortening

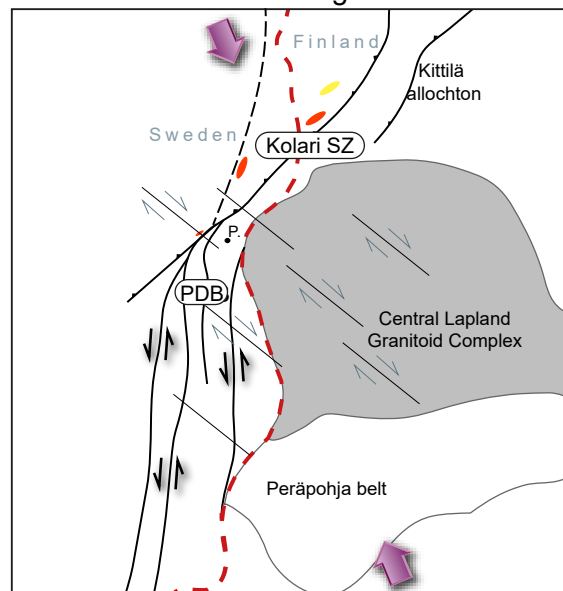


Figure 13. Map sketches of the three main deformation stages affecting the Pajala deformation belt (PDB) and the Kolari shear zone (Kolari SZ). Purple arrows indicate direction of crustal shortening. Red and yellow ellipsoids indicate Fe and Cu-Au deposits, respectively. Red dashed line indicate national border.

CONCLUSIONS

Structural geological mapping combined with 3D geological modelling in the Pajala area has provided insights into the complex deformation pattern associated with the Pajala deformation belt (PDB) and the Kolari shear zone. Several major shear zones related to the PDB were accurately mapped and their sense of shearing determined. Strike and dip measurements were then combined with subsurface geometries obtained from gravity and resistivity models. The overall interpretations reveal a wedge-shaped subsurface geometry for the Pajala Deformation Belt directly south of Pajala with steeply east-dipping shear zones along its western border (Koijuvaara shear zone) and steeply west-dipping shear zones towards the east. Mylonites associated with these shear zones record multi-reactivations, accommodating reverse, dextral, oblique and sinistral movements. The internal part of the wedge is folded, resulting in multiple ellipsoidal dome structures, often surrounded by a network of N–S-striking shear zones. The larger domes were possibly formed by interference of NW–SE-orientated F1 folds and N–S-orientated F2 folds, or resulted from vertical extrusion operating during a single deformation event. Fold interference patterns occur to the west of the PDB (e.g. Nunasvaara and Masugnsbyn areas; see Lynch et al., 2018, Grigull et al., 2018), forming large-scale, oblate or sub-circular dome-like structures. Within the PDB, however, most domes appear strongly elongated in a N–S direction, suggesting E–W flattening and possible vertical extrusion as important deformation mechanisms. Consequently, the PDB is interpreted as a 60 to 80 km wide transpressive wedge formed during NE–SW transpressive shortening (D1), followed by E–W shortening (D2). D2 eventually resulted in an eastward offset of the PDB along the NE–SW-striking Kolari Shear zone north of Pajala. These shear zones should therefore not be treated as part of the same shear systems. Time constraints on D2 are based on the relatively young metamorphic ages (1.8 Ga) recorded in the PDB in comparison with its surroundings (1.84 Ga). Folding of the metamorphic fabrics during D2 must therefore have occurred after 1.8 Ga. Finally, deformation by NNW–SSE shortening (D3) caused discrete faulting and sinistral brittle-ductile reactivation along the PDB's western boundary.

REFERENCES

- Bergman, S., Kübler, L. & Martinsson, O., 2001: Description of regional geological and geophysical maps of northern Norrbotten County (east of the Caledonian orogen). *Sveriges geologiska undersökning Ba 56*, 110 pp.
- Bergman, S., Billström, K., Persson, P.-O., Skiöld, T. & Evins, P., 2006: U-Pb age evidence for repeated Palaeoproterozoic metamorphism and deformation near the Pajala shear zone in the northern Fennoscandian shield. *GFF 128*, 7–20.
- Berthelsen, A. & Marker, M., 1986: 1.9-1.8 Ga old strike-slip megashears in the Baltic Shield, and their plate tectonic implications. *Tectonophysics 128*, 163–181.
- Eriksson, T., 1954: Pre-Cambrian geology of the Pajala district, northern Sweden. *Sveriges geologiska undersökning C 522*, 38 pp.
- Gerdin, P., Johansson, L., Hansson, K.-E., Holmqvist, A. & Ottosson, D., 1990: Grafit-uppslagsgenerering i Norrbotten. *Unpublished report, SGAB PRAP 90068*, 77 pp.
- Grigull, S., Berggren, R. & Jönsson, C., 2014: Summary report on the geological and geophysical characteristics of the Käymjärvi-Ristimella key area. *Sveriges geologiska undersökning SGU-rapport 2014:30*.
- Grigull, S. & Berggren, R., 2015: Geological and geophysical fieldwork in the Käymjärvi-Ristimella key area. *SGU-rapport 2015:29*. Sveriges geologiska undersökning.
- Grigull, S., Berggren, R., Jönberger, J., Jönsson, C., Hellström, F.A. & Luth, S., 2018: Folding observed in Palaeoproterozoic supracrustal rocks in northern Sweden. *In: Bergman, S. (ed): Geology of the Northern Norrbotten ore province, northern Sweden. Rapporter och Meddelanden 141*, Sveriges geologiska undersökning. This volume pp 205–257.
- Johansson, L., 1985: Liviövaara, geofysisk tolkning, *SGAB Prospekteringsrapport PRAP 85092*, 3 pp.
- Jonsson, E. & Kero, L., 2013: Beskrivning till berggrundskartorna 27M Korpilombolo NV, NO, SV, SO och 27N Svanstein NV, SV. *Sveriges geologiska undersökning K 391–394*, 20 pp.
- Kärki, A., Laajoki, K. & Luukas, J., 1993: Major Palaeoproterozoic shear zones of the central Fennoscandian Shield. *Precambrian Research 64*, 207–223.
- Ladenberger, A., Andersson, M., Smith, C. & Carlsson, M., 2018: Till geochemistry in northern Norrbotten – regional trends and local signature in the key areas. *In: Bergman, S. (ed): Geology of the Northern Norrbotten ore province, northern Sweden. Rapporter och Meddelanden 141*, Sveriges geologiska undersökning. This volume pp 401–428.
- Lahtinen, R., Korja, A., & Nironen, M., 2005: Paleoproterozoic tectonic evolution. *Developments in Precambrian Geology, 14*, 481–531.
- Lahtinen, R., Huhma, H., Lahaye, Y., Jonsson, E., Manninen, T., Lauri, L.S., Bergman, S., Hellström, F., Niiranen, T. & Nironen, M., 2015: New geochronological and Sm–Nd constraints across the Pajala shear zone of northern Fennoscandia: Reactivation of a Paleoproterozoic suture. *Precambrian Research 256*, 102–119.
- Leever, K., Gabrielsen, R., Sokoutis, D. & Willingshofer, E., 2011: The effect of convergence angle on the kinematic evolution of strain partitioning in transpressional brittle wedges: Insight from analog modelling and high-resolution digital image analysis. *Tectonics 30*, TC2013, doi:10.1029/2010TC002823.
- Luth, S. & Jönsson, C., 2014: Barents Project 2014: Summary report on the geological and geophysical characteristics of the Liviöjärvi key area. *SGU-rapport 2014:29*, Sveriges geologiska undersökning. 34 pp.
- Luth, S., Jönsson, C. & Jönberger, J., 2015: Barents Project 2014: Integrated geological and geophysical field studies in the Liviöjärvi key area, Pajala region. *SGU-rapport 2015:12*, Sveriges geologiska undersökning. 29 pp.
- Lynch, E.P., Hellström, F.A., Huhma, H., Jönberger, J., Persson, P.-O. & Morris, G.A., 2018: Geology, lithostratigraphy and petrogenesis of c. 2.14 Ga greenstones in the Nunasvaara and Masugnsbyn areas, northernmost Sweden. *In: Bergman, S. (ed): Geology of the Northern Norrbotten ore province, northern Sweden. Rapporter och Meddelanden 141*, Sveriges geologiska undersökning. This volume pp 19–77.
- Martinsson, O., 2004: Geology and metallogeny of the northern Norrbotten Fe-Cu-Au Province. *Society of Economic Geologists Guidebook Series 33*, 131–148.

- Martinsson, O. & Wanhainen, C., 2013: The northern Norrbotten ore district. *In*: O. Martinsson & C. Wanhainen (eds.): Fe oxide and Cu-Au deposits in the northern Norrbotten ore district. Excursion guidebook SWE5, 12th Biennial SGA Meeting, Uppsala, Sweden, 19–28.
- Martinsson, O., Bergman, S., Persson, P.-O., Schöberg, H., Billström, K. & Shumlyansky, L., 2018: Stratigraphy and ages of Palaeoproterozoic metavolcanic and metasedimentary rocks at Käymäjärvi, northern Sweden. *In*: Bergman, S. (ed): Geology of the Northern Norrbotten ore province, northern Sweden. *Rapporter och Meddelanden 141*, Sveriges geologiska undersökning. This volume pp 79–105.
- Niiranen, T., Poutiainen, M. & Mänttari, I., 2007: Geology, geochemistry, fluid inclusion characteristics, and U–Pb age studies on iron oxide–Cu–Au deposits in the Kolari region, northern Finland. *Ore Geology Reviews 30*, 75–105.
- Niiranen, T., Nykänen V., Lahti, I. & Karinen, T., 2009: Geological interpretation of the upper crust along the FIRE 4A and 4B seismic profiles. *Geologian tutkimuskeskus, arkistoraportti, K 31.4/2009/78*
- Niiranen, T., 2011: IOCG and Porphyry-Cu deposits in northern Finland and Sweden. *Excursion guide, 25th International Applied Geochemistry Symposium 22-26 August 2011 Rovaniemi, Finland.*
- Nironen, M., 1997: The Svecofennian Orogen: a tectonic model. *Precambrian Research 86*, 21–44.
- Padget, P., 1977: Beskrivning till berggrundskartbladen Pajala NV, NO, SV, SO. *Sveriges geologiska undersökning Af 21–24*, 73 pp.
- Tikoff, B. & Peterson, K., 1998: Physical experiments of transpressional folding. *Journal of Structural Geology Vol. 20 nr. 6*, 661–672.
- Väisänen, M., 2002: Structural features in the central Lapland greenstone belt, northern Finland. 20 s. *Geologian tutkimuskeskus, arkistoraportti, K 21.42/2002/3.*



Geological Survey of Sweden
Box 670
SE-751 28 Uppsala
Phone: +46 18 17 90 00
Fax: +46 18 17 92 10
www.sgu.se

Uppsala 2018
ISSN 0349-2176
ISBN 978-91-7403-393-9
Tryck: Elanders Sverige AB